

Chapter 8

FIELD EFFECTS OF OVERHEAD TRANSMISSION LINES AND STATIONS

by D. W. Deno and L. E. Zaffanella

8.1 INTRODUCTION

Overhead transmission lines and stations generate electric and magnetic fields, which are taken into consideration as part of the overall design characteristics. The advent and increasing use of higher voltage lines has increased the relative importance of field effects such as induced voltages and currents in conducting bodies. This, in turn, has prompted increased activity in the following areas: the calculation and measurement techniques for electric and magnetic fields; the calculation and measurement of induced currents and voltages on objects of different shapes for all line voltages and design configurations; the calculation and measurement of currents and voltages induced in people as a result of different induction mechanisms; the investigation of the sensitivity of people to different field effects; and the study of conditions resulting in fuel ignition, corona from grounded objects, and other possible field effects.

This chapter describes the design rules developed as a result of research programs conducted at Project UHV. Whenever possible, the field effects were defined in terms of currents, voltages, and energies induced in conductive bodies placed in proximity to transmission lines or stations. Possible effects related to the long-term exposure of people, animals, and vegetation were not the object of research programs at Project UHV; electrical, rather than biological, investigations were performed. Biological research is the object of other programs sponsored by EPRI and various organizations at other research centers. Consequently, only a brief review of the status of biological research is presented. The chapter does present considerable new material on the subject of electric- and magnetic-field effects. The material reflects the increased amount of information made available in the past few years as a result of the great interest in resolving the issues related to the subject. An extensive section on different methods to reduce the electric field of transmission lines has been added to this edition. Magnetic-field effects are also treated more extensively in this edition, but most of the chapter is devoted to electric-field effects because it is the electric field rather than the magnetic field that becomes of increasing concern as transmission-line voltages are increased.

8.2 ELECTRIC AND MAGNETIC FIELDS: DEFINITIONS

PHASORS AND VECTORS

The concepts of phasors and vectors need to be clarified because they are used frequently in this chapter to describe electric and magnetic fields. A vector is described by a magnitude and an angle in space, whereas a phasor is a quantity with a sinusoidal time variation described by a magnitude and an angle in time. The space components of a vector may be phasors of different time angles. These complex vectors occur in fields around three-phase transmission lines and stations. A vector is indicated with an arrow over a capital letter (\vec{E}), and a phasor with a wave sign over a capital letter (\tilde{E}) or with sinusoidal functions of time [$e(t)$].

ELECTRIC FIELD

Electric field is a vector field of electric-field strength (E -field) defined by its space components along three orthogonal axes. For steady-state sinusoidal fields, each space component is a phasor that may be expressed by a rms value (V/m) and a phase as in

$$\vec{E} = e_x(t) \vec{u}_x + e_y(t) \vec{u}_y + e_z(t) \vec{u}_z \quad (8.2.1)$$

where $\vec{u}_x, \vec{u}_y, \vec{u}_z$ are the unit vectors along the x, y, and z axes and $e_x(t), e_y(t), e_z(t)$ are phasors, functions of time as shown in Eq. 8.2.2 for the x-space component:

$$e_x(t) = E_x \cos(\omega t + \phi_x) = E_{x,r} \cos \omega t + E_{x,i} \sin \omega t \quad (8.2.2)$$

where E_x is the magnitude and ϕ_x the phase angle of $e_x(t)$, and $E_{x,r}$ and $E_{x,i}$ are the real and imaginary parts.

It is also useful to visualize the vector, \vec{E} , expressed by Eq. 8.2.1 as a vector moving in space. It can be shown that this vector rotates in a plane and describes an ellipse. The maximum field strength occurs along the major axis of the ellipse. The length of the semi-axis represents the value of the maximum field strength. A quarter period later, the field is in the direction of the minor axis, and the length of the semi-axis represents its magnitude. The field in the direction perpendicular to the plane of the ellipse is zero.

MAGNETIC FIELD

The magnetic flux density, (B), rather than the magnetic-field strength, ($H = B/\mu$), is used to describe the magnetic-field generated by currents in the conductors of transmission lines. Thus, magnetic field is defined as a vector field of magnetic flux density (B -field). The vector properties of the B -field are the same as those described for the E -field. The magnitudes of the space components are expressed by their rms values. The International System unit (S.I.) is the tesla (T), which is one weber per square meter (Wb/m^2). The gauss (G) is the commonly used unit. One tesla is equal to 10^4 G.

FREQUENCY

Frequency is the number of complete cycles of sinusoidal variations per unit time. Electric- and magnetic-field space components have a fundamental frequency equal to that of the transmission voltage. For ac transmission, the frequency is 60 Hz in the United States, Brazil, Canada, and Mexico, and 50 Hz in most other countries.

HARMONIC CONTENT

Harmonic content is the distortion of sinusoidal waveform characterized by indication of the magnitude and order of the Fourier series terms describing the wave. The harmonic content of the electric field coincides with that of the line voltage, and the harmonic content of the magnetic field coincides with that of the line current for single-phase systems. For power transmission lines, the harmonic content is small, except during transient conditions, and of little concern for the purpose of field measurements except at points near large industrial loads such as saturated power transformers, n -pulse rectifiers, or aluminum and chlorine plants where certain harmonics may reach 10% of the line voltage. Laboratory installations may also have voltage or current sources with significant harmonic content.

MAXIMUM VALUE OF THE ELECTRIC (MAGNETIC) FIELD

The maximum value of the electric (magnetic) field is the rms value of the maximum space component of the electric field. Its direction is the major axis of the field ellipse.

UNPERTURBED FIELD

The field in the vicinity of an object may be perturbed by the presence of the object. Unperturbed field is the field that is present when the object is removed. Because the electric field at or close to the surface of an object is generally strongly perturbed, the value of the unperturbed electric field is often used to characterize the intensity of electric-field effects of transmission lines and stations. The magnetic field is not generally perturbed by the presence of objects that are free of magnetic materials.

SINGLE-PHASE AND THREE-PHASE FIELDS

A single-phase electric (magnetic) field is generated by conductors energized by a single-phase source of alternating voltage (current). All the field components are in phase. The field at any point may be described in terms of its time-varying magnitudes and invariant direction.

Three-phase transmission lines and stations generate three-phase fields with space components not in phase. The field is de-

scribed by the field ellipse, i.e., by magnitude and direction of the major and minor semi-axes.

When the minor semi-axis is much smaller (less than 10%) than the major semi-axis, the field may be practically considered single-phase. This occurs close to boundary surfaces, such as ground. The induction on long objects in a three-phase field also requires the consideration of the phase difference between the major semi-axes of the field ellipses in different points along the objects.

UNIFORM FIELD

A region has a uniform field if, in all points of the region, the magnitude and direction of the field are constant.

VERTICAL COMPONENT OF THE ELECTRIC FIELD

The vertical component of the electric field under a transmission line is the rms value of the component of the electric field along the vertical line passing through the point of measurement. This quantity is often used to characterize induction effects in objects close to ground level.

SPACE POTENTIAL

The space potential of a point is a phasor representing the voltage difference between that point and ground. The space potential is perturbed by the introduction of an object in the field. Unperturbed space potential, which exists if the object is removed, is often used.

8.3 CALCULATION OF ELECTRIC FIELDS

GENERAL METHOD FOR TRANSMISSION LINES

Electric fields in proximity to ac transmission lines are calculated assuming that there is no free charge in space. The earth is assumed to be a perfect conductor because the time required for charges to redistribute on the earth surface under the action of a change in applied field (relaxation time, $\tau = \rho \epsilon$) is extremely small (0.1 to 100 nanoseconds) compared to the period of the power frequency. The permittivity of air is practically independent of weather conditions and is equal to the permittivity of free space,

$$\epsilon = 8.854 \cdot 10^{-12} \text{ F/m}$$

Each conductor of a transmission line, including wires at ground potential, must be characterized by a real and imaginary voltage, $V = V_r + jV_i$, and by diameter. For regular bundle conductors and for calculation of fields far from the conductor surface, it is convenient to consider the equivalent single conductor having a diameter, d_{eq} , given by

$$d_{eq} = D \sqrt[n]{\frac{nd}{D}} \quad (8.3.1)$$

where D is the bundle diameter, n is the number of subconductors, and d is the diameter of the subconductors. For nonregular bundles, the equivalent diameter is calculated as the diameter of the single conductor with the same total charge. For such calculation, it is sufficient to assume a single-phase energization of the bundle.

The charges, Q , on the conductors are determined through the voltages, V , and the Maxwell potential coefficients, P , with the matrix equation

$$[Q] = [P]^{-1} [V] \quad (8.3.2)$$

Equation 8.3.2 is written for both real and imaginary charges:

$$[Q] = [Q_r] + j [Q_i] \quad (8.3.3)$$

$$[Q_r] = [P]^{-1} [V_r] \text{ and } [Q_i] = [P]^{-1} [V_i] \quad (8.3.4)$$

For a transmission line composed of parallel conductors (a, b, \dots) above a perfectly flat ground plane, the elements of the matrix, $[P]$, are given by equations such as Eq. 8.3.5 and Eq. 8.3.6:

$$P_{aa} = \frac{1}{2\pi\epsilon} \ln \left(\frac{4y_a}{d_a} \right) \quad (8.3.5)$$

$$P_{ab} = \frac{1}{2\pi\epsilon} \ln \left[\frac{(x_a - x_b)^2 + (y_a + y_b)^2}{(x_a - x_b)^2 + (y_a - y_b)^2} \right]^{1/2} \quad (8.3.6)$$

where y_a and y_b are the heights of conductors a and b above ground, d_a is the diameter of conductor a , and x_a and x_b are the horizontal coordinates of conductors a and b .

Once Eq. 8.3.2 is solved and the charges on each conductor are known, the electric field at a point, N , of coordinates (x_N, y_N) in space may be calculated. The field due to the charge on conductor a and to its image inside the earth is

$$\vec{E}_a = \vec{E}_{x,a} \vec{u}_x + \vec{E}_{y,a} \vec{u}_y \quad (8.3.7)$$

where \vec{u}_x and \vec{u}_y are the unit vectors along the horizontal and vertical axes and $E_{x,a}$ and $E_{y,a}$ are given by

$$\begin{aligned} \vec{E}_{x,a} &= \frac{(q_{ra} + j q_{ia})(x_N - x_a)}{2\pi\epsilon [(x_a - x_N)^2 + (y_a - y_N)^2]} \\ &\quad - \frac{(q_{ra} + j q_{ia})(x_N - x_a)}{2\pi\epsilon [(x_a - x_N)^2 + (y_a + y_N)^2]} \end{aligned} \quad (8.3.8)$$

and

$$\begin{aligned} \vec{E}_{y,a} &= \frac{(q_{ra} + j q_{ia})(y_N - y_a)}{2\pi\epsilon [(x_a - x_N)^2 + (y_a - y_N)^2]} \\ &\quad - \frac{(q_{ra} + j q_{ia})(y_N + y_a)}{2\pi\epsilon [(x_a - x_N)^2 + (y_a + y_N)^2]} \end{aligned} \quad (8.3.9)$$

The horizontal and vertical components, \tilde{E}_x and \tilde{E}_y , of the electric field are calculated by adding the contributions of all the conductors (a, b, \dots):

$$\tilde{E}_x = \tilde{E}_{x,a} + \tilde{E}_{x,b} + \dots \quad (8.3.10)$$

and

$$\tilde{E}_y = \tilde{E}_{y,a} + \tilde{E}_{y,b} + \dots \quad (8.3.11)$$

Each of these components is a phasor, expressed by real and imaginary parts:

$$\tilde{E}_x = \tilde{E}_{rx} + j \tilde{E}_{ix} \quad (8.3.12)$$

and

$$\tilde{E}_y = \tilde{E}_{ry} + j \tilde{E}_{iy} \quad (8.3.13)$$

Equations 8.3.12 and 8.3.13 completely describe the electric field. Instead of using the horizontal and vertical components, the electric field may be described by the real part vector and the imaginary part vector:

$$\vec{E}_r = E_{rx} \vec{u}_x + E_{ry} \vec{u}_y \quad (8.3.14)$$

and

$$\vec{E}_i = E_{ix} \vec{u}_x + E_{iy} \vec{u}_y \quad (8.3.15)$$

Both representations are shown in Figure 8.3.1. In Figure 8.3.1 the field vector coincides with the real vector, \vec{E}_r (space angle 57°), for a phase angle equal to zero and with the imaginary vector, \vec{E}_i (space angle -59°), for a phase angle equal to 90° electrical degrees. In this example the vector rotates clockwise. When the vector is in the direction of the major axis of the ellipse, it coincides with the maximum field, \vec{E}_{\max} . As the vector

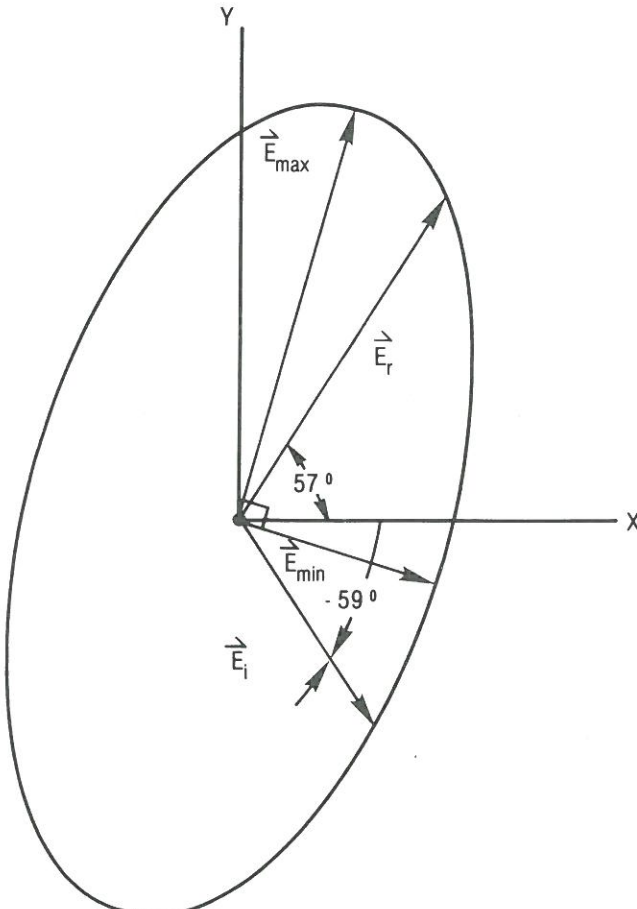


Figure 8.3.1. Example of electric-field ellipse at a point in space.

rotates, its projections on the horizontal and vertical axes will describe the horizontal and vertical components. It should be noted that the maximum values of these components *do not coincide* with instantaneous vectors but with the projections of the rotating vector at some instants during the cycle. Methods to calculate magnitude and direction of the semi-axes of the field ellipse are described in Appendix 8.1.

The space potential at a point, N , of coordinates x_N and y_N may be evaluated starting from the conductor charges $[Q_r] + j [Q_i]$ evaluated previously.

The potential due to the charge of conductor a is

$$V_{N,a} = \frac{q_{ra} + j q_{ia}}{2\pi\epsilon} \ln \frac{\sqrt{(x_a - x_N)^2 + (y_a - y_N)^2}}{y_a} - \frac{q_{ra} + j q_{ia}}{2\pi\epsilon} \ln \frac{\sqrt{(x_a - x_N)^2 + (y_a + y_N)^2}}{y_a} \quad (8.3.16)$$

The space potential is due to all the conductors, (a, b, \dots) and is

$$V_N = V_{N,a} + V_{N,b} + \dots = V_{rN} + j V_{iN} \quad (8.3.17)$$

LATERAL PROFILE OF ELECTRIC FIELD AT GROUND LEVEL

The calculation of the electric field of a transmission line at ground level is a considerable simplification of the general method of field calculation. In fact, the electric field on a flat horizontal ground may be represented by a vertical vector. The field at a point, N , on the ground due to the charge, q_a , on conductor a and to its image, $-q_a$, in the ground (see Figure 8.3.2) is calculated using Eq. 8.3.9 with $y_N = 0$:

$$\tilde{E}_a = \frac{q_{ra} + j q_{ia}}{2\pi\epsilon} \cdot \frac{2y_a}{(x_a - x_N)^2 + y_a^2} \quad (8.3.18)$$

where q_{ra} and q_{ia} are the real and the imaginary parts of the charge on conductor a calculated with Eq. 8.3.4 and $(x_a - x_N)$ is the horizontal distance between conductor a and the point, N , where the field is calculated.

The total field at point N is obtained summing the contributions of all the conductors (a, b, c, \dots):

$$\tilde{E} = \tilde{E}_a + \tilde{E}_b + \tilde{E}_c + \dots \quad (8.3.19)$$

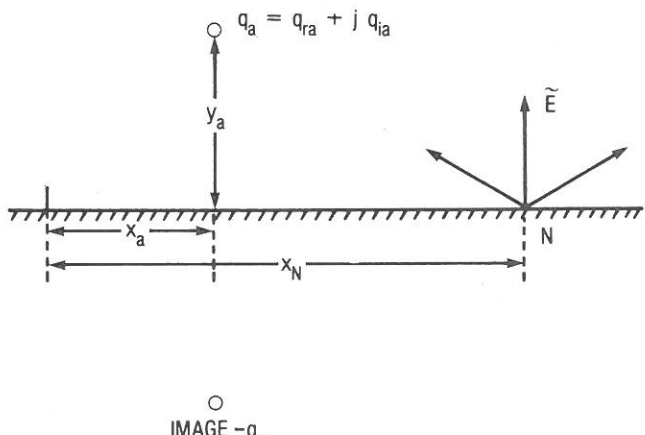


Figure 8.3.2. Electric field at ground caused by a conductor line charge.

Equation 8.3.19 expresses a phasor:

$$\tilde{E} = E_r + j E_i \quad (8.3.20)$$

The magnitude of the electric field is

$$E = \sqrt{E_r^2 + E_i^2} \quad (8.3.21)$$

and the phase angle, θ , is

$$\theta = \arctan \frac{E_i}{E_r} \quad (8.3.22)$$

If the calculation of the electric field at ground is repeated at different points in a section perpendicular to the transmission line, the lateral profile of the transmission-line electric field is obtained. Unless otherwise specified, the lateral profile is calculated at the section where the line has the lowest clearance to ground.

Examples of calculated lateral profiles are shown in Figure 8.3.3. Particularly important for line design are the maximum field and the field at the edge of the transmission corridor. The maximum field occurs within the transmission corridor even though, for flat configurations, it might occur slightly outside the outer phases.

MAXIMUM ELECTRIC FIELD AT GROUND—GENERALIZED CURVES

Figures 8.3.4–8.3.7 show universal curves using nondimensional quantities that may be used to calculate the maximum electric field at ground for different single-circuit line geometries.

The use of Figure 8.3.4 is illustrated in the following example computation of the maximum electric field at ground for a single-circuit line with $V = 525$ kV, a 3×3.3 -cm conductor bundle with 45-cm spacing, phase-to-phase distance $S = 10$ m, and height of the center of the bundle to ground $H = 10.6$ m. The equivalent bundle diameter (Eq. 8.3.1) is $D = 0.3$ m. For

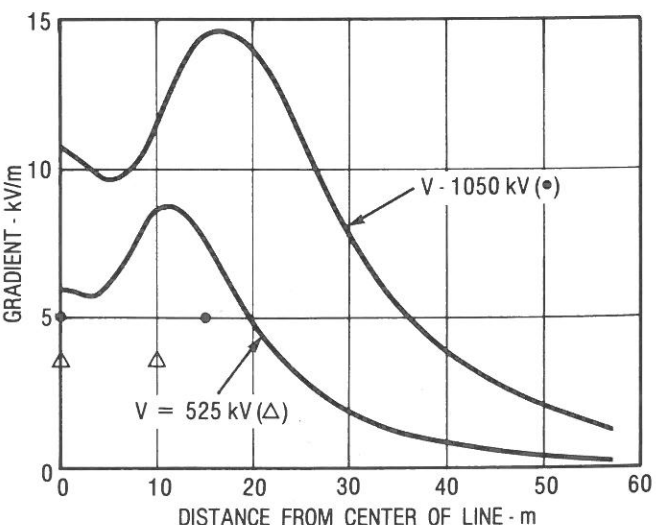


Figure 8.3.3. Lateral profiles of electric field at ground. (a) Line at 525 kV with 3×3.3 -cm conductor, 45-cm spacing, spaced 10 m, and 10.6 m above ground, flat configuration. (b) Line at 1050 kV with 8×3.3 -cm conductors on 101-cm diameter, spaced 18.3 m, and 18.3 m above ground, flat configuration.

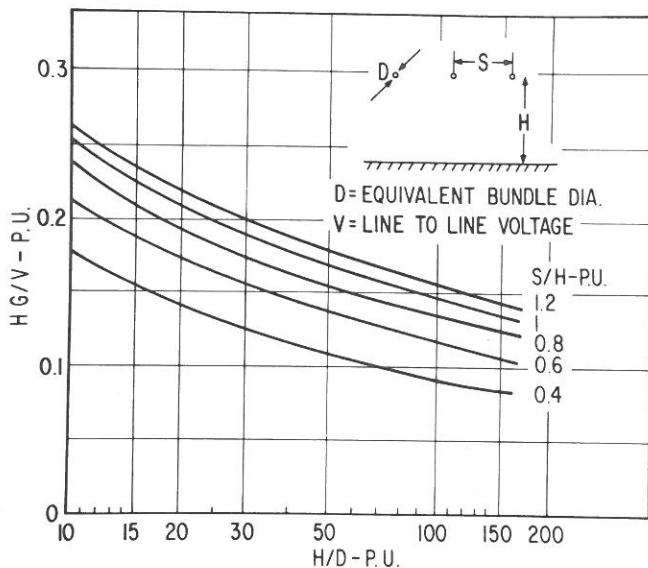


Figure 8.3.4. Universal curves to calculate the maximum electric field at ground, E , for lines of flat configuration. H is the height to the center of the bundle.

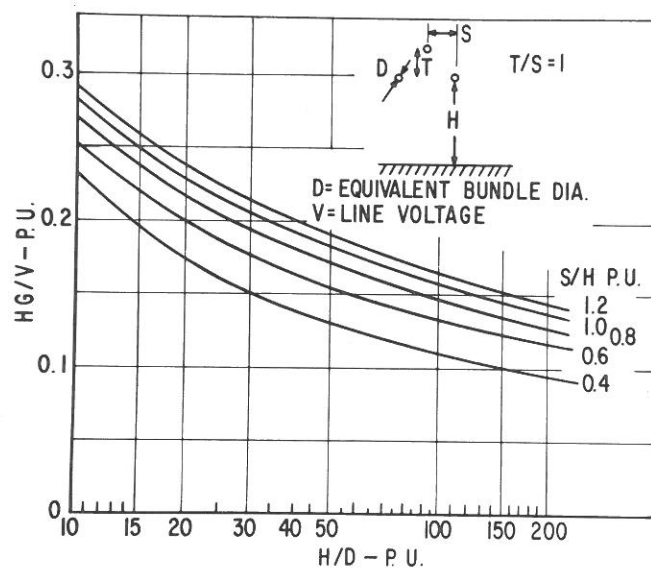


Figure 8.3.6. Universal curves to calculate the maximum electric field at ground, E , for lines of triangular configuration with $T/S = 1$. H is the height to the center of the bundle.

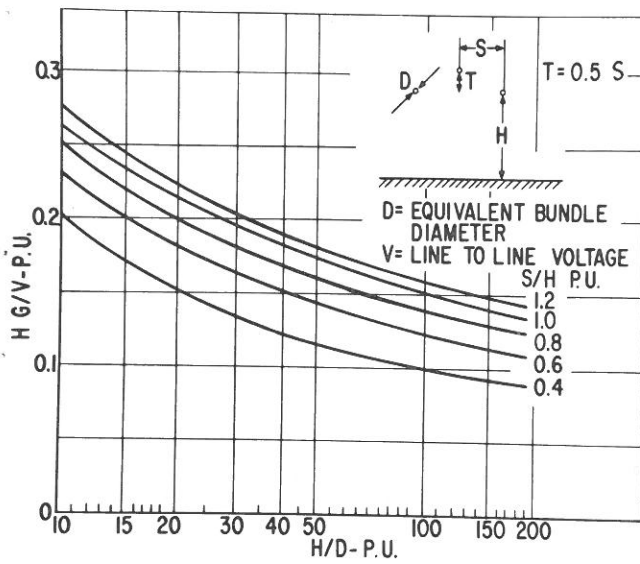


Figure 8.3.5. Universal curves to calculate the maximum electric field at ground, E , for lines of triangular configuration with $T/S = 0.5$. H is the height to the center of the bundle.

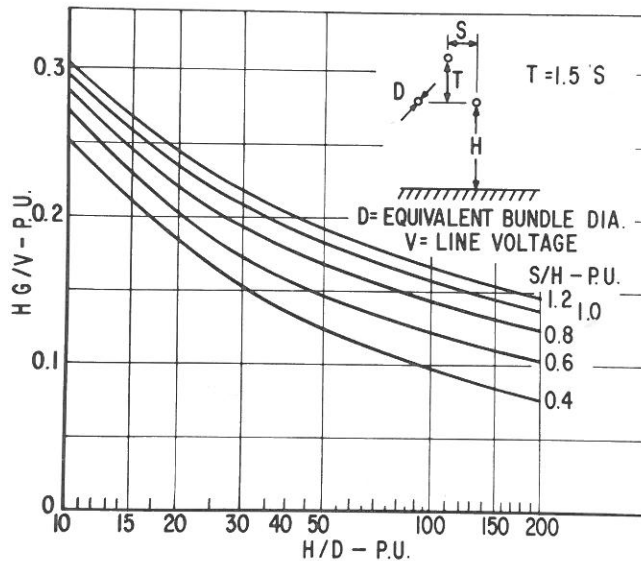


Figure 8.3.7. Universal curves to calculate the maximum electric field at ground, E , for lines of triangular configuration with $T/S = 1.5$. H is the height to the center of the bundle.

$H/D = 10.6/0.3 = 35.3$ and $S/H = 10/10.6 = 0.94$, Figure 8.3.4 gives $HE/V = 0.179$. The maximum field at ground is $E = 0.179 \times 525/10.6 = 8.8 \text{ kV/m}$, which is confirmed in Figure 8.3.3. Figures 8.3.4–8.3.7 do not consider the presence of overhead ground wires, which have a negligible effect on the field at ground (see next subsection).

EFFECT OF CHANGES IN LINE GEOMETRY

The electric field at ground in the vicinity of a transmission line is a function of its geometrical parameters. Therefore, field effects may be minimized to some extent by appropriate line design. Some changes in line design may affect the electric field under or close to the line (where the maximum field exists) dif-

ferently from the electric field outside the transmission corridor. The following parameters are considered: line configuration, height, sag, conductor dimensions, phase spacing, and shield wires.

Line Configuration: Figure 8.3.8 shows electric field profiles for three different line configurations: flat, equilateral delta, and vertical.

Voltage, phase spacing, conductor diameter, and clearance to ground are the same in the three cases. The maximum electric field at ground is lowest for the equilateral delta configuration and highest for the vertical and flat configurations. For non-equilateral delta configurations, the field profile is between that

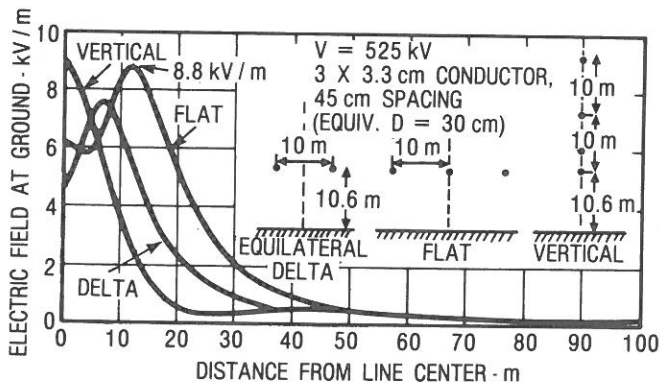


Figure 8.3.8. Lateral profiles of the electric field at ground for lines of flat, equilateral delta, and vertical configurations.

of the flat and the equilateral delta. The electric field outside the transmission corridor is extremely low for lines with vertical configuration and is highest for lines with flat configuration. It should be noted, however, that vertical lines require the tallest towers.

Line Height: Increasing line height is the most effective line design change to reduce the maximum field at ground. However, increasing line height requires the use of taller or more frequent towers. The effect of line height on the maximum field cannot be easily observed in the curves of Figures 8.3.4–8.3.7. The vertical-axis variable of the figures implies an inverse proportionality between height, H , and field, E . However, H is contained also in the horizontal-axis variable and in the parameter S/H . The relation between H and E may be expressed by the empirical equation

$$\left(\frac{E_1}{E_2}\right) = \left(\frac{H_1}{H_2}\right)^m \quad (8.3.23)$$

where E_1 and E_2 are the maximum fields for lines of minimum heights H_1 and H_2 , respectively. The value of m depends on the geometry. For $S/H = 1$ and $S/D = 33$, $m \approx -1.4$ for three-phase lines of flat configuration, and $m \approx -1.6$ for three-phase lines of equilateral delta configuration. For instance, assume that the maximum field of a line with flat configuration is 8.8 kV/m for a 10.6-m height above ground. An increase of 1 m, to a height of 11.6 m, will reduce the maximum field to

$$E_2 \approx 8.8 \left(\frac{11.6}{10.6}\right)^{-1.4} = 7.8 \text{ kV/m} \quad (8.3.24)$$

The field at ground outside the transmission corridor is influenced in a completely different way by a change in line height. An example is shown in Figure 8.3.9. An increase in the line height causes a decrease in the field up to a critical distance, L_c , from the line center but causes an increase in the field at distances greater than L_c . Thus, raising line height is not desirable if concern is for the electric field outside the transmission-line corridor.

The critical distance, L_c , at which a change in line height does not cause a change in electric field is a function of the line parameters as shown in Figure 8.3.10 for three-phase lines of horizontal configuration. The following example shows how the dimensionless curves of Figure 8.3.10 may be used. Consider the horizontal configuration described in Figure 8.3.8 for which $S/H = 0.94$ and $S/D = 33$. Figure 8.3.10 gives a value of $L_c/S = 2.5$, and therefore $L_c = 2.5 \times 10 = 25 \text{ m}$ (82 ft).

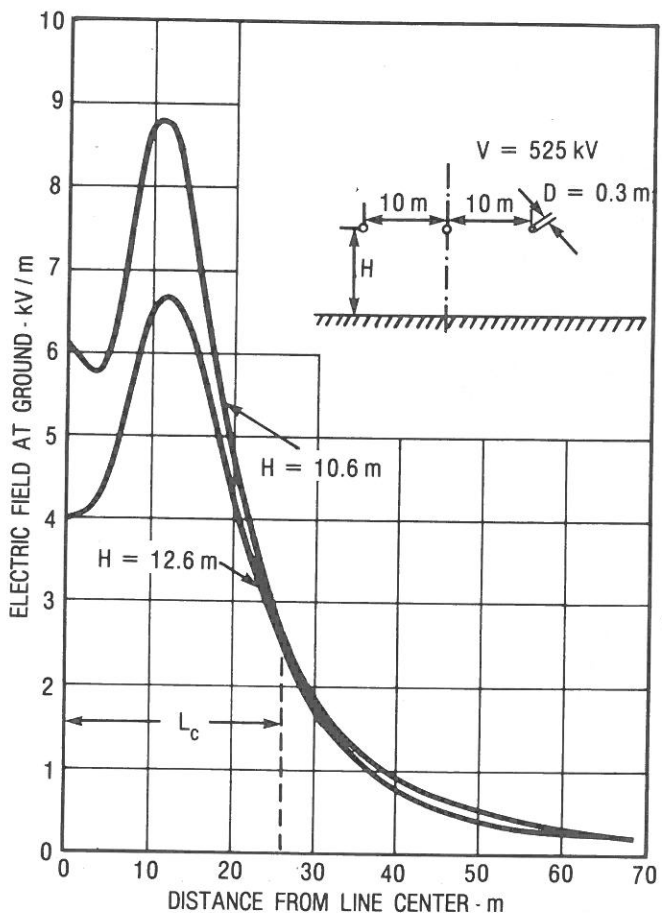


Figure 8.3.9. Example of the effect of a change in line height on the electric field at ground level. At the critical distance, L_c , no change in electric field magnitude occurs.

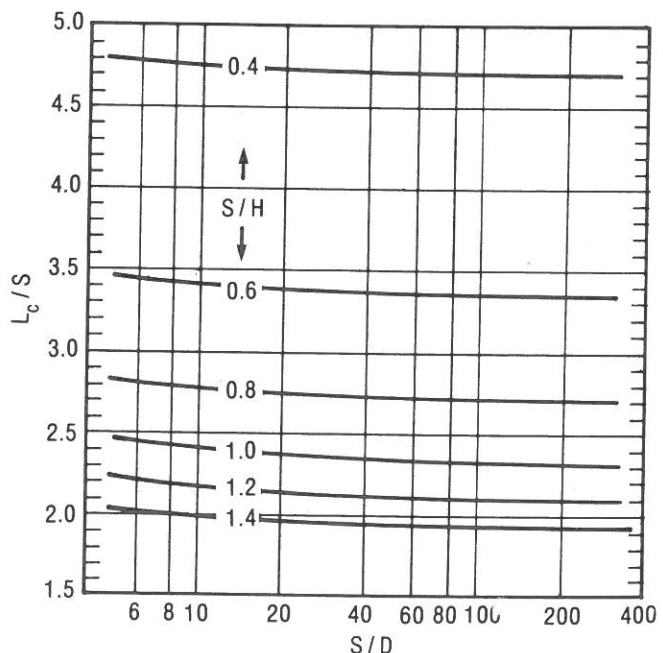


Figure 8.3.10. Critical distance, L_c , at which there is no change in electric field at ground for a change in line height. L_c is measured horizontally from line center.

As a corollary of the preceding discussion, the field outside the transmission corridor is generally greater toward the towers than at midspan (neglecting the shielding effect of the towers).

Sag: The effect of sag is normally neglected if the lateral profile is taken at the lowest point of the catenary. In this case, the difference in the calculations of the electric field at ground with and without account of the sag is less than $\pm 1\%$ within the transmission corridor. This difference, expressed as a percentage of the field, increases with the distance from the line but in absolute values is always negligible. For instance, for the 550-kV flat line configuration of Figure 8.3.3, the field at 76 m (250 ft) from the line center of the midspan cross section, calculated accounting for the sag, is 128 V/m, which is 10%, or 12 V/m, higher than the field calculated without taking the sag into account, which is 116 V/m. This calculation required three-dimensional techniques and was carried out for an example in which the sag was 16.8 m (55 ft). The effect of sag is negligible also for lateral profiles at other cross sections along the span up to a distance from the tower equal to one-third of the span. Closer to the tower, however, the lateral profile at ground may be significantly different from that calculated with Eqs. 8.3.18–8.3.22, taking as line height the height at the cross section where the profile is calculated. For instance, in the example of Figure 8.3.3 with a sag of 16.8 m (55 ft), the lateral profile at the tower (neglecting the tower shielding effect) is close to that calculated using a height above ground of 23.7 m (78 ft) instead of using the real height at the tower, which is 27.4 m (90 ft).

Conductor Dimensions: The effect of conductor dimensions may be evaluated using, in the case of bundles, the equivalent conductor diameter expressed by Eq. 8.3.1. In fact, by definition, this is the diameter of the single conductor that would have the same total electric charge per unit of length as the bundle and therefore would cause essentially the same field at ground. Figures 8.3.4–8.3.7 show the effect of D on the maximum field at ground. The effect of D on the field outside the transmission corridor is practically the same as the effect on the maximum field, i.e., in all points the electric field, E , changes proportionally to the charges on the conductors. For three-phase lines, the dependence of the field at ground on the diameter of the conductors may be expressed by the approximate equation

$$\frac{E_1}{E_2} \approx \frac{\ln(2S/D_2)}{\ln(2S/D_1)} \quad (8.3.25)$$

where E_1 and E_2 are the electric fields at ground for lines of phase spacing S and diameters D_1 and D_2 , respectively. Using Eq. 8.3.25, the effect of diameter may be easily verified. For instance, assume the field at a point close to ground is equal to 5 kV/m with a bundle of two conductors, $d = 3.8$ cm (1.5 in), spaced 46 cm (18 in), and a phase spacing of 9.15 m (30 ft). The equivalent diameter is 18.7 cm according to Eq. 8.3.1. A change to a single conductor with $d = 5.1$ cm (2 in) results in a field equal to

$$E = 5 \frac{\ln \frac{18.3}{0.187}}{\ln \frac{18.3}{0.051}} = 3.9 \text{ kV/m} \quad (8.3.26)$$

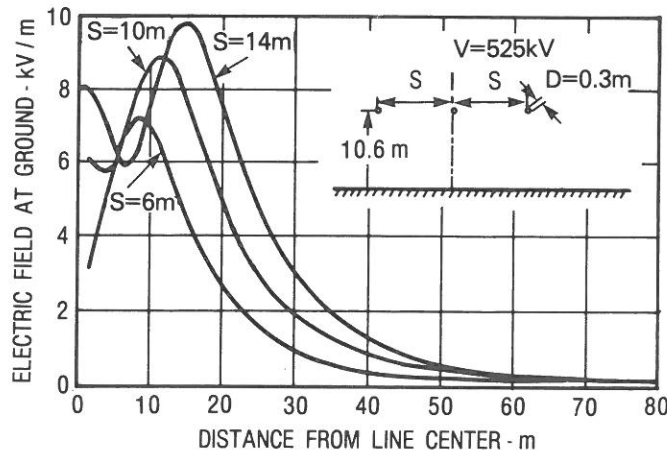


Figure 8.3.11. Examples of the effect of phase spacing on the electric field at ground level.

The preceding example shows that drastic changes in conductor dimensions are required to appreciably affect the field at ground level. These changes are not always among the available options because of cost, corona, or other reasons.

Phase Spacing: The effect of phase spacing on maximum gradient at ground may be evaluated using Figures 8.3.4–8.3.7. More compact lines produce lower electric field at ground. This effect is shown more clearly in Figure 8.3.11 for a line of flat configuration. Therefore, EHV line compaction is very attractive for purposes of field reduction. Therefore, EHV line compaction may require towers without metallic members between phases and may cause a deterioration of the line corona performance. Therefore, a reduction in phase spacing that reduces the field at ground might require larger, or more, conductors to avoid an increase in radio and audible noise.

Shield Wires: Practically, shield wires for lightning protection do not influence the electric field at ground level. Their presence causes a reduction of the electric field at ground that is no greater than 1–2% because the shield wires are above the phase conductor, farther away from ground.

ELECTRIC FIELD OF DOUBLE-CIRCUIT LINES

Computation of electric field at ground level for double circuits may be made using the general method described previously. It is more difficult to use generalized curves because additional geometrical variables are necessary. Furthermore, the phasing of both circuits greatly influences the voltage gradients at ground. Figure 8.3.12 shows the electric-field lateral profile for an example of a 525-kV, double-circuit line and different phase arrangements. Figure 8.3.13 shows an example of a 345-kV, double-circuit line with a different basic geometry. Phase arrangements 1 and 5 are the superbundle and the low-reactance arrangements mentioned in Chapter 3, respectively. The superbundle arrangement corresponds to the lowest electric field at the conductor and to the highest electric field at ground, whereas the low-reactance arrangement corresponds to the highest electric field at the conductor and to the lowest electric field at ground. The electric field for one single circuit energized and the second circuit grounded is described by curve 6 in Figures 8.3.12 and 8.3.13. In this case, the electric field is intermediate between

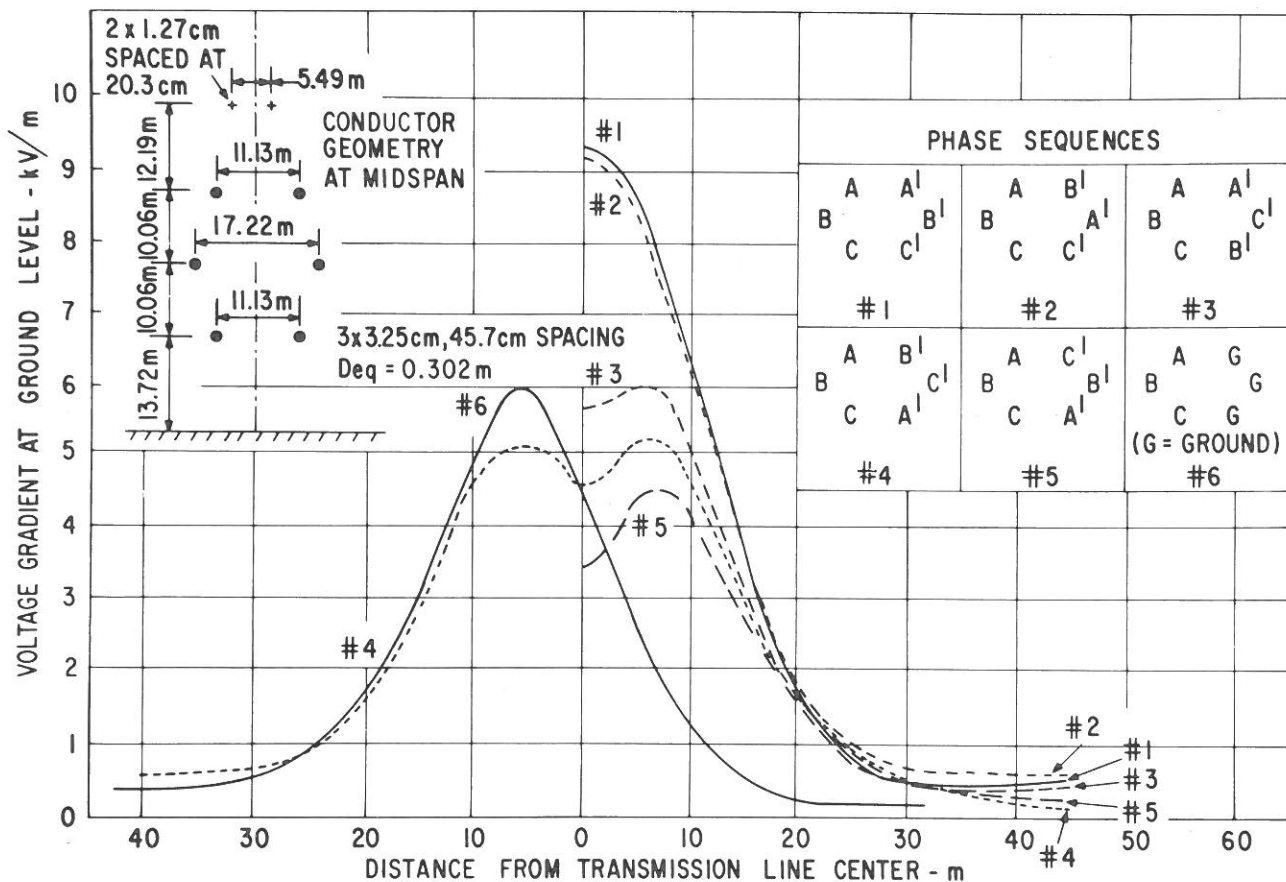


Figure 8.3.12. Electric field at ground level for a typical double-circuit geometry and different phase arrangements. $V = 525 \text{ kV}$. Phase arrangement 1, superbundle, corresponds to the maximum ground gradient (and the minimum conductor gradient). Phase arrangement 5, low-reactance, corresponds to the minimum ground gradient (and the maximum conductor gradient and maximum power transfer capability).

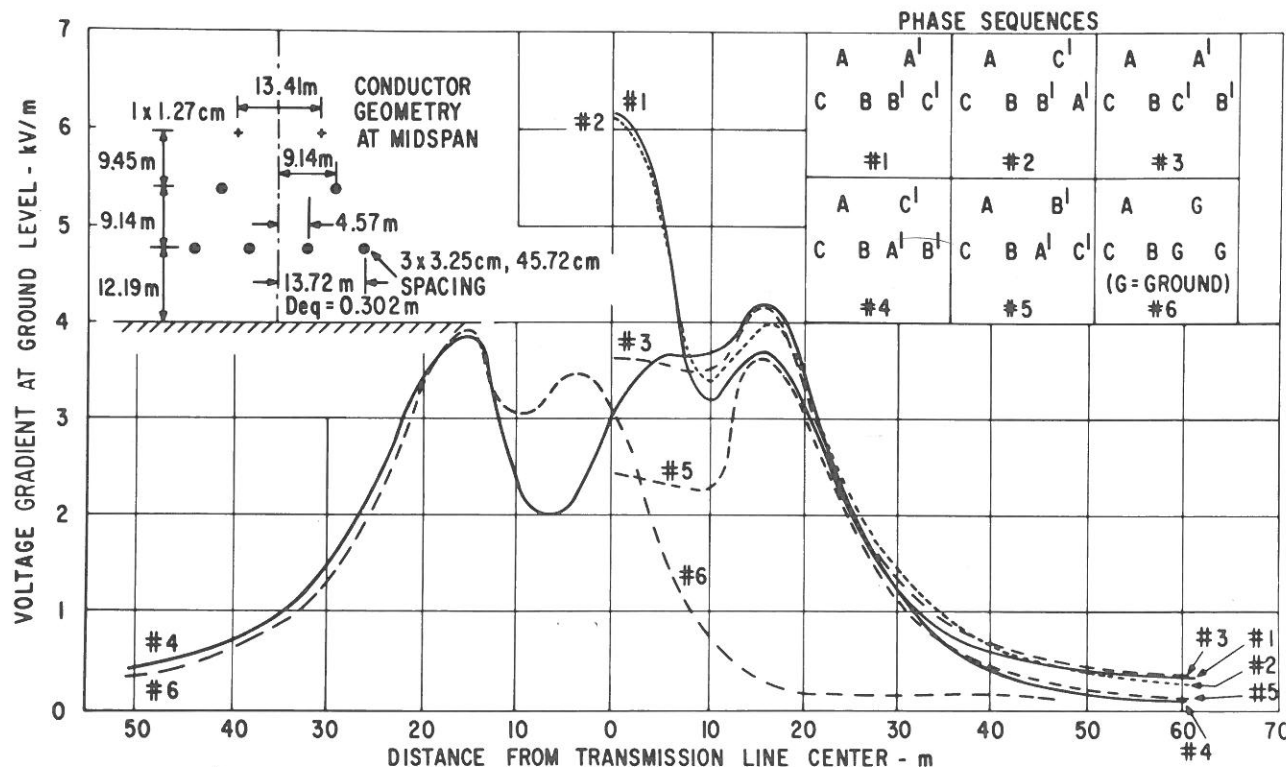


Figure 8.3.13. Electric field at ground level for a typical double-circuit geometry and different phase arrangements. $V = 345 \text{ kV}$.

that for the low-reactance arrangement and that for the superbundle arrangement. All the curves in Figures 8.3.12 and 8.3.13 were computed accounting for the ground wires. Their influence, however, was found to be negligible.

Generalized curves giving the maximum electric field at ground level were computed for the two basic geometries represented in Figures 8.3.12 and 8.3.13. The phase arrangements considered are the superbundle (case 1 in Figures 8.3.12 and 8.3.13), the low-reactance (case 5), and the single circuit (case 6). In the case of the single circuit, a slight difference exists if the deenergized circuit is considered as floating instead of grounded. If the deenergized circuit is floating, generalized curves will be found in Figure 8.3.14 for the double-circuit arrangement of Figure 8.3.12, and in Figure 8.3.6 for the double-circuit arrangement of Figure 8.3.13.

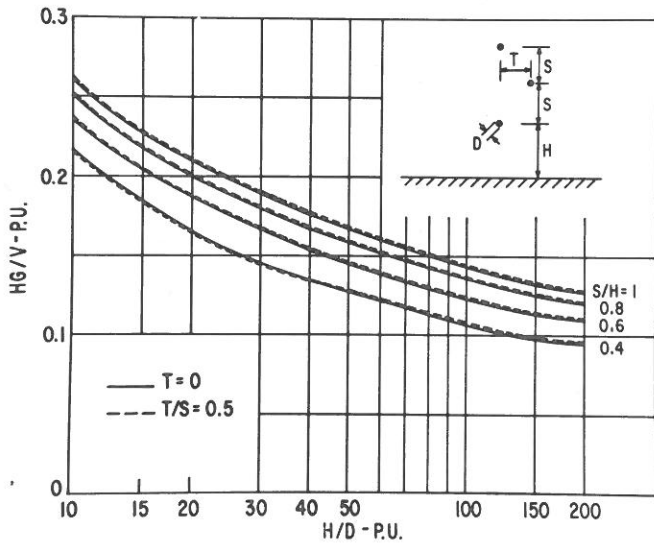


Figure 8.3.14. Generalized curves for the computation of maximum electric field at ground level. Single circuit with vertical phase arrangement.

Figure 8.3.14 shows that the distance, T , has little effect on the maximum electric field at ground level. This was verified also for the other double-circuit arrangement of Figure 8.3.12, so that, for this case, generalized curves could be traced considering $T = 0$ (vertical arrangements of each circuit).

The generalized curves for the superbundle arrangement are given in Figure 8.3.15. The generalized curves for the low-reactance arrangement are given in Figure 8.3.16. For the geometry of Figure 8.3.13, the generalized curves were computed fixing the parameter, Δ (see Figure 8.3.17), within such limits that its influence would be negligible. The generalized curves for the low-reactance arrangement are given in Figure 8.3.17. The generalized curves for the superbundle arrangement are given in Figure 8.3.18. With the help of the generalized curves described previously, the maximum electric field could be directly comput-

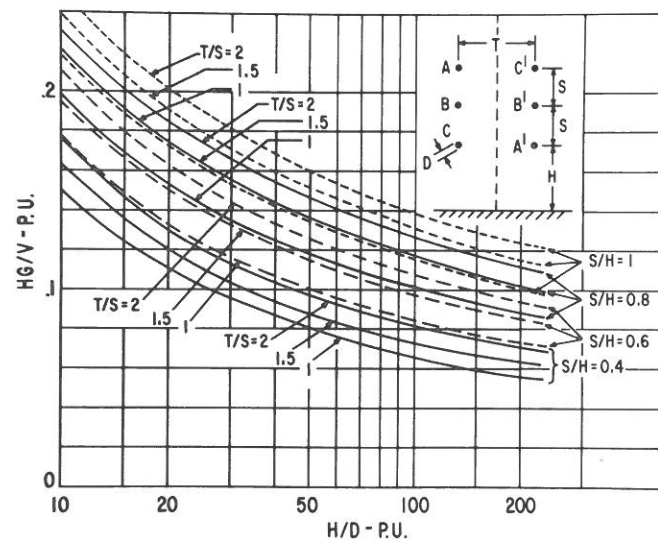


Figure 8.3.16. Generalized curves for the computation of maximum electric field at ground level. Double-circuit geometry of the type of Figure 8.3.12, low-reactance phase arrangement.

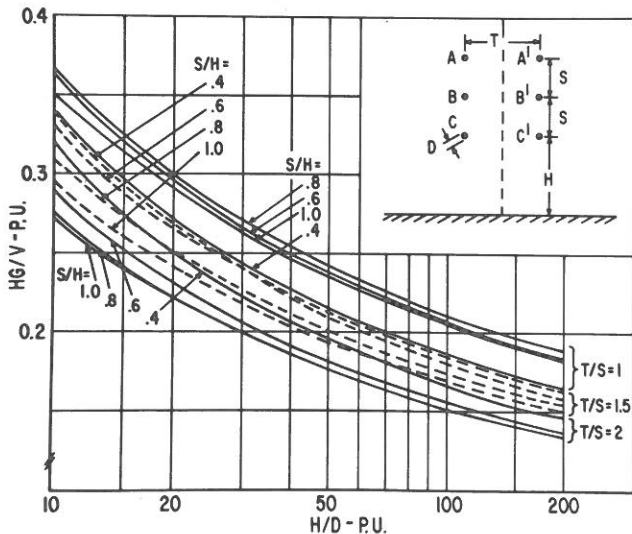


Figure 8.3.15. Generalized curves for the computation of maximum electric field at ground level. Double-circuit geometry of the type of Figure 8.3.12, superbundle phase arrangement.

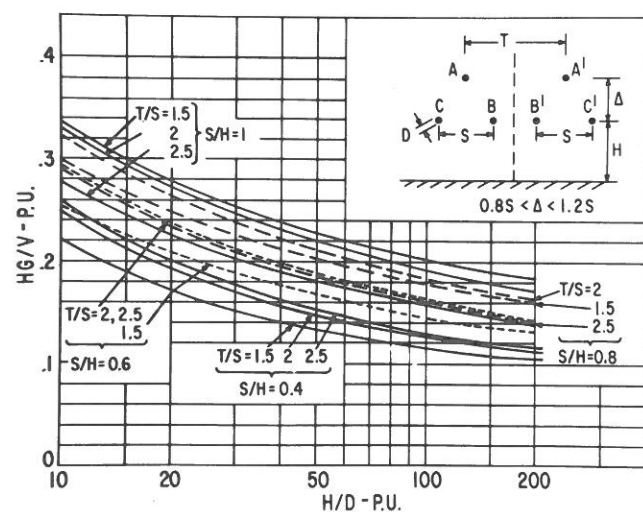


Figure 8.3.17. Generalized curves for the computation of maximum electric field at ground level. Double-circuit geometry of the type of Figure 8.3.13, low-reactance phase arrangement.

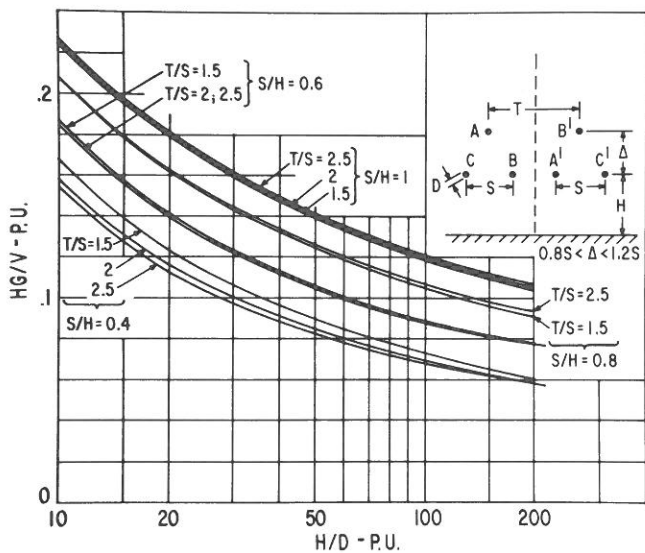


Figure 8.3.18. Generalized curves for the computation of maximum electric field at ground level. Double-circuit geometry of the type of Figure 8.3.13, superbundle arrangement.

ed for a wide variety of line geometries and for the two extreme phase arrangements. For other phase arrangements, good approximation is achieved by computing the electric field for superbundle and low-reactance arrangements assuming a similarity with respect to Figures 8.3.12 and 8.3.13.

As an example, consider a geometry of the type of Figure 8.3.12 with phase arrangement 3 and the following parameters:

$$\begin{aligned} V &= 765 \text{ kV} \\ d_{eq} &= 42.5 \text{ cm} \\ H &= 15.1 \text{ m} \\ S &= 12 \text{ m} \\ T &= 13.4 \text{ m} \end{aligned}$$

For the superbundle arrangement (Figure 8.3.15), with $H/D = 32$, $T/S = 1.1$, and $S/H = 0.8$, $HE/V = 0.258$ is obtained, and therefore $E = 13 \text{ kV/m}$. Similarly, for the low-reactance arrangement (Figure 8.3.16), $E = 6.9 \text{ kV/m}$ is obtained. The ratio of the superbundle to low-reactance maximum gradient values $13/6.9 = 1.88$ is close to that of Figure 8.3.12 ($9.3/4.5 = 2.05$). Therefore, approximate values for phase arrangement 3 may be obtained assuming that the proportionality between maximum electric fields, 9.3 kV/m and 6 kV/m for configurations 1 and 3 of Figure 8.3.12, is maintained:

$$E_{\max 3} = \frac{6}{9.3} \times 13 = 8.4 \text{ kV/m} \quad (8.3.27)$$

An analysis of the electrostatic effects on long objects that are nonparallel to transmission lines requires the evaluation of the electric field at different distances from the center of the line both in amplitudes and in phase. The evaluation of the phase angle is made using Eq. 8.3.22. An example of phase angle computations is given in Figure 8.3.19 in which the phase angle of the voltage gradient at ground level is shown for the double-circuit geometry of Figure 8.3.13 and a phase arrangement that is a mirror image of case 3.

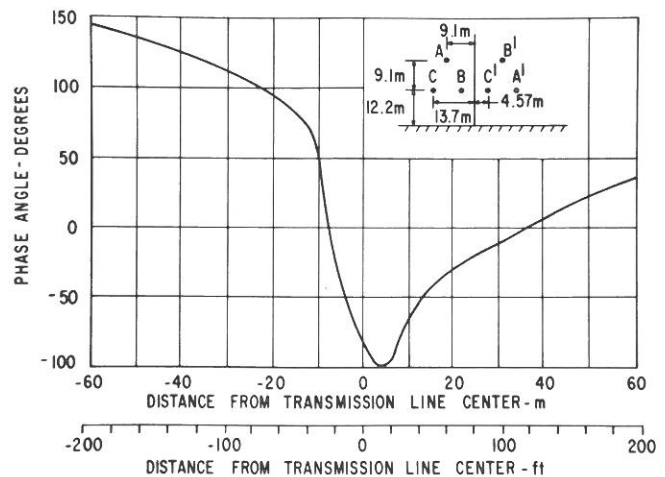


Figure 8.3.19. Phase angle of electric field at ground level for a mirror image of case 3 of Figure 8.3.13. Angles are referred to phase A of the transmission line.

ELECTRIC FIELD AT LINE BENDS

Line bends change the calculation of electric fields from the traditional two-dimensional analysis to a much more difficult three-dimensional problem. A 60-Hz air model, described in Appendix 8.3, was used at Project UHV to evaluate correction factor curves.

In the study of line bends it is practical to use a dimensionless correction factor, k , defined as

$$E_b = k E_g \quad (8.3.28)$$

where E_b is the field at ground at the line bend and E_g is the corresponding value when the line is straight. The field is described in terms of a well-known field, that of a straight transmission line. Any deviation of the factor, k , from 1 is attributed to the bend. Utilizing test data, factors were evaluated for the 45° and 90° bends. The 90° bend definitions are given in Figure 8.3.20 with correction factors shown in Figure 8.3.21. The 45° bend definitions are given in Figure 8.3.22 with correction factors shown in Figure 8.3.23.

The field at two or more phase spacings from the line center is increased inside the bend and decreased outside it. However, the field within the right-of-way increases on the outer part of the bend. It should be noted that the highest field does not occur at the point of the highest correction factor. The strongest fields were measured at a distance equal to three-fourths of the phase spacing from the center toward the outer phase along the bisector of the bend.

ELECTRIC FIELD IN SUBSTATIONS

Basically, electric field effects in substations will be of the same nature as those close to transmission lines. Induced currents and spark discharges will depend on the particular situation and on the intensity of the field. Also, for substations, electric field at ground level is a useful parameter for characterizing the intensity of the electric field.

In designing new substations, the electric field of existing substations is a useful reference. The electric field at ground may be described by means of equifield contour lines traced on the substation map. An example of such contours in a switchyard

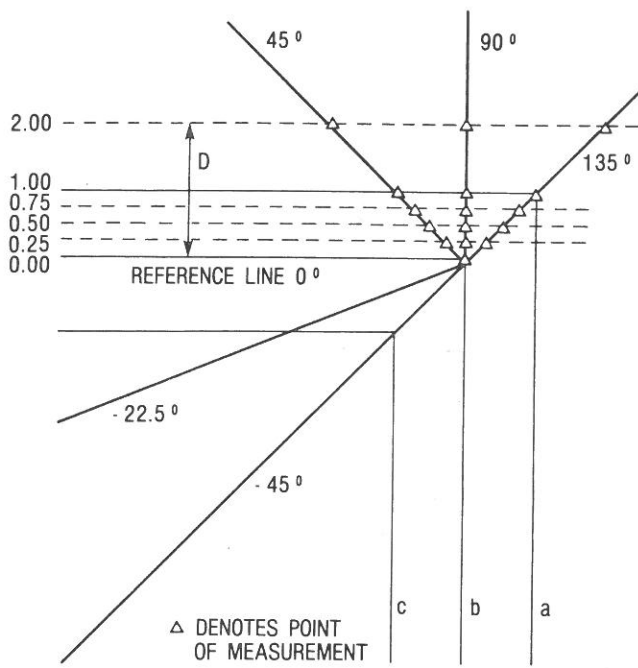


Figure 8.3.20. Plan view of a 90° line bend. Measured data along the bisector of the bend at angles of -45° and 135° are shown in Figure 8.3.21.

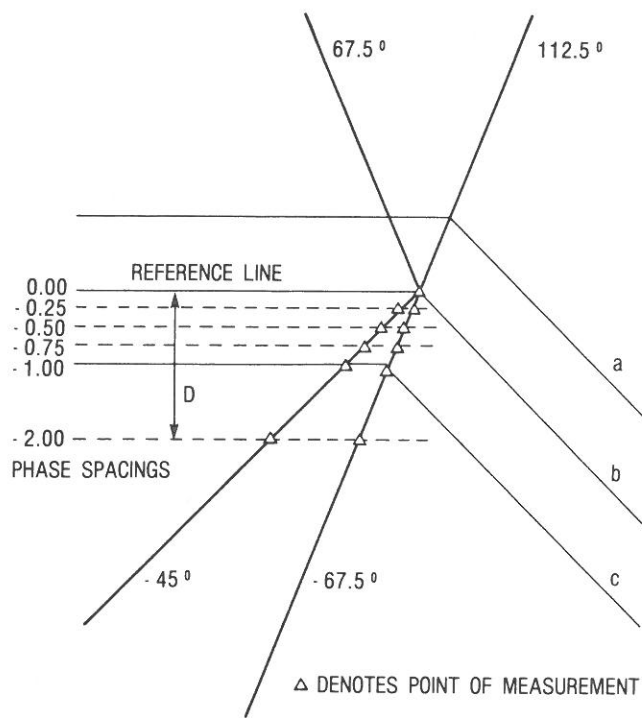


Figure 8.3.22. Plan view of a 45° line bend. Measurements along the bisector of the bend at angles of -67.5° and 112.5° are shown in Figure 8.3.23.

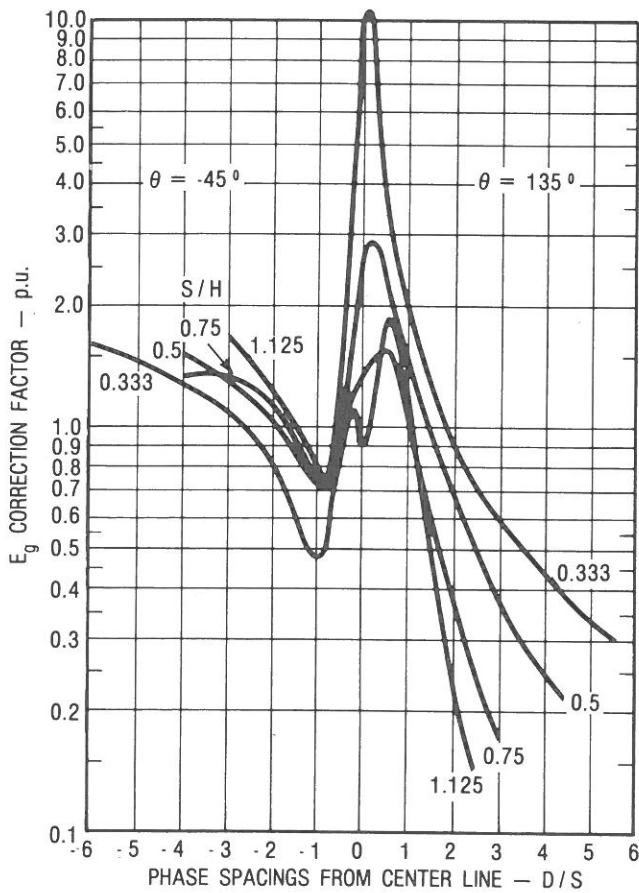
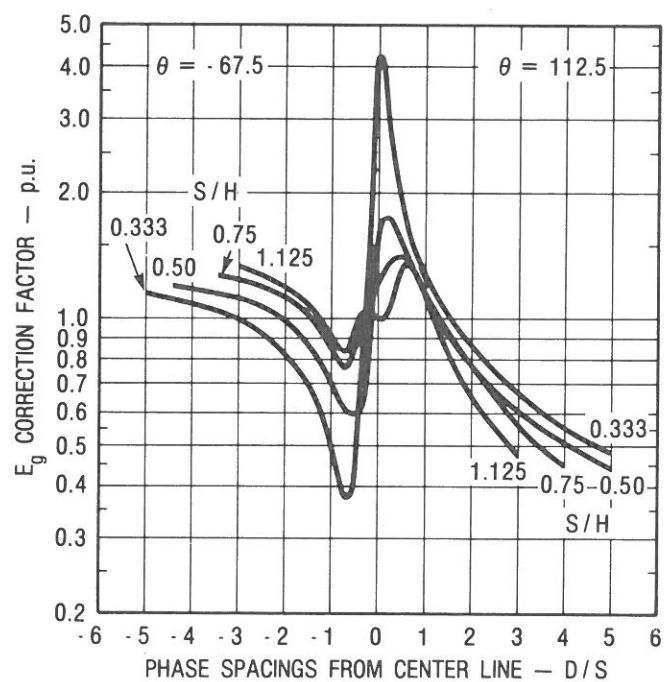


Figure 8.3.21. Correction factor (ratio between field with bend and field without bend) at different points along the bisector of the line bend. Height above ground equal to 50 equivalent bundle diameters.



with a voltage of 520 kV line-to-line is shown in Figure 8.3.24. The measurements were taken one meter above the ground. The maximum electric field measured was 8.5 kV/m. Typically, electric fields of 2 kV/m were measured close to breakers and disconnects between the phases, whereas values close to 6 kV/m

were measured off the outside phase, where access roads or walk areas might be present. Working areas usually have a low electric field. If the breaker heads are deenergized for servicing, the fields around the heads will appear to be lower unless they are close to an energized overhead bus.

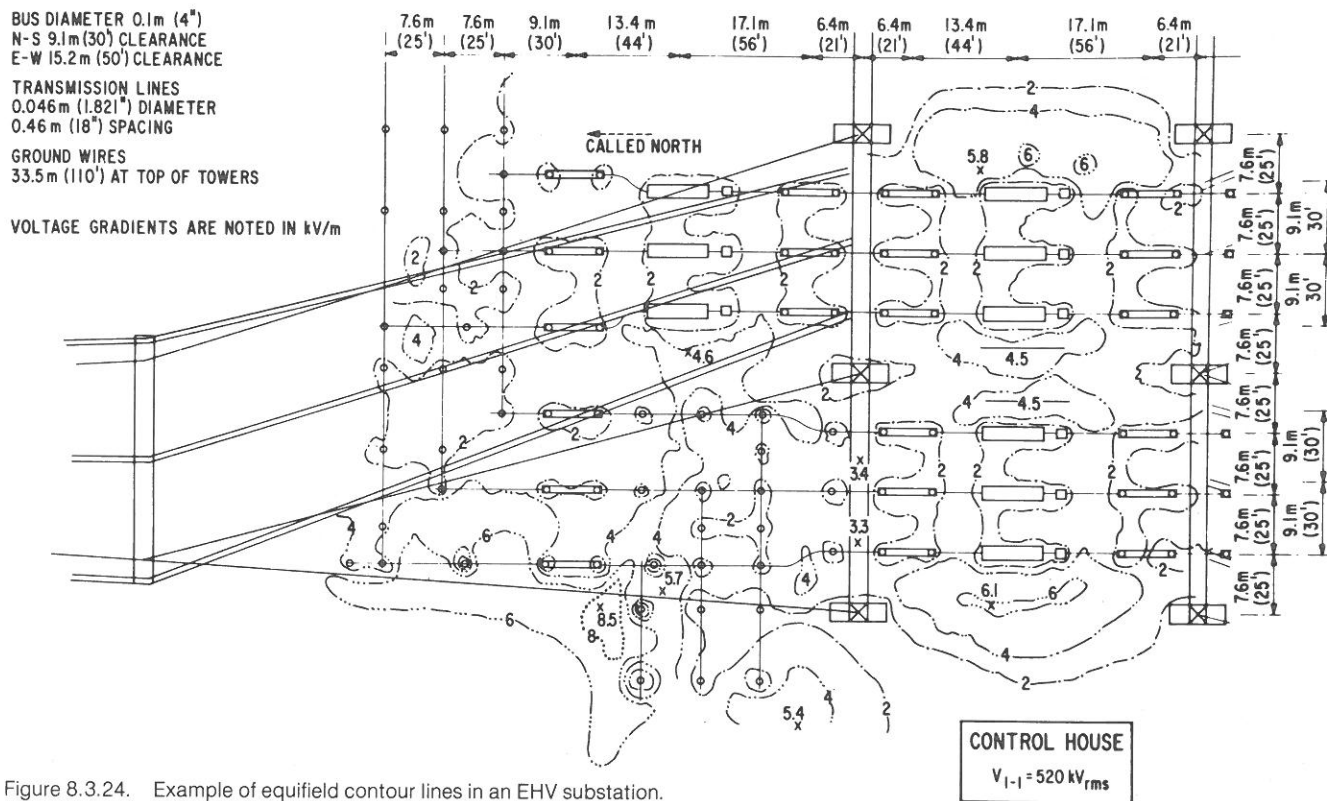


Figure 8.3.24. Example of equifield contour lines in an EHV substation.

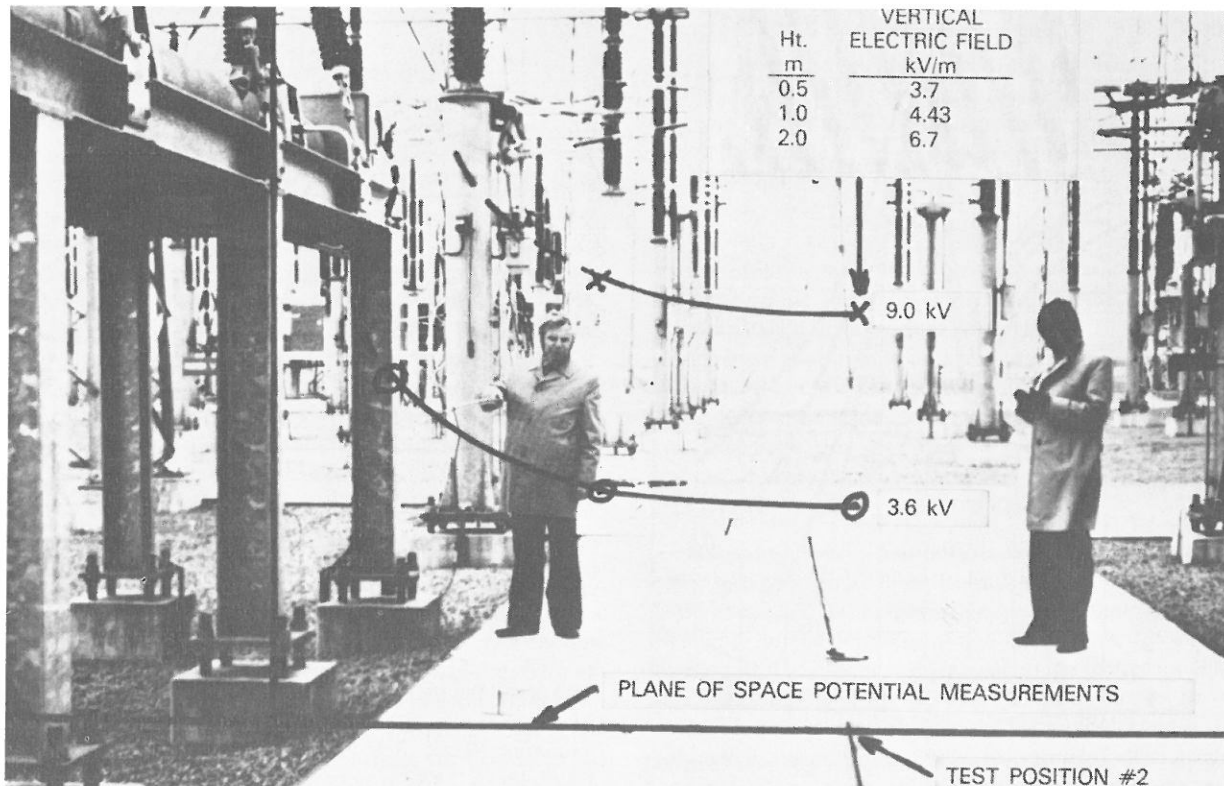


Figure 8.3.25. Example of measurements of space potential in an EHV substation.

The electric field about the substation structure shown in Figure 8.3.24 is very nonuniform. All of the support structures shield the field at ground level. Figure 8.3.25 gives examples of vertical electric field measurements in an EHV station.

Table 8.3.1
VOLTAGE GRADIENTS AT GROUND LEVEL
MEASURED IN EHV SUBSTATIONS

| Voltage # (kV) | Measured Gradient (kV/m) | Gradient Off Outer Phase* (kV/m) | Bus Height (m) | Geometrical Characteristics | |
|-------------------|--------------------------------|--|----------------------|--------------------------------|-------------------------|
| | | | | Phase Spacing (m) | Base Height** (m) |
| 345 | 7.5 | 6.5 | 7 | 4.5 | 4.0 |
| 520 | 8.5 | 6.0 | 9 | 7.5 | 5.0 |
| 765 | 9.0 | 8.5 | 12 | 15.6 | 6.5 |

* Representative maximum gradients encountered along the bus far from terminations and discontinuities

** Height of the grounded base supporting insulating elements (posts, measuring devices, switches, breakers)

Line-to-line

The maximum values and the substation characteristics for three typical substations are listed in Table 8.3.1. The values of the third column in Table 8.3.1 may be computed if the equivalent diameters of the buses and of the grounded bases are known. Generally, the highest values of field are encountered close to breaker heads. Therefore, breaker head dimensions are important for the computations. If the value of the electric field is of concern in the preliminary design stages of EHV and UHV substations, it is suggested that the maximum ground level electric field be evaluated for any geometry using the curves of Figure 8.3.26. The curves of this figure are computed using non-dimensional ratios between geometrical and electrical quantities. V is the phase-to-phase voltage. The equivalent diameters of the buses and of the grounded bases are assumed equal to $H/24$ where H is the bus height. This criterion yields a value of $D = 0.5$ m if $H = 12$ m. If no base is present, the curves of Figure 8.3.4 may be used. The use of Figure 8.3.26 is illustrated by the following example.

Consider a 1200-kV substation with an insulation distance, $H-B$, equal to 7 m, and a phase spacing, S , equal to 18 m. The maximum gradient at ground will then depend on the bus height. For $H = 15$ m ($S/H = 1.2$, $B/H = 0.53$), Figure 8.3.26 gives $HG/V = 0.128$ and $G = 0.128 \times 1200/15 = 10.2$ kV/m. For $H = 18$ m ($S/H = 1$, $B/H = 4.5$), the maximum gradient is $G = 0.116 \times 1200/18 = 7.75$ kV/m.

The maximum gradient occurs at a distance of a few meters off the outer phase. The gradients at ground level may be reduced by designing substations with large values of bus height. Simpler procedures, however, will produce the same effect. For instance, grounded wires strung off the outer phases at a height above ground equal to the base height will easily reduce the field at ground level by a factor of two or more depending on the number and separation of the wires.

Whenever there is a question concerning the electric field in a substation, the easiest solution is to measure the field. Measurements of personnel exposure are discussed in Section 8.10. If the substation has yet to be built, then measurements in similar substations will provide the electric field values to be reported. For any unusual situation, an air model may provide detailed information on electric-field intensity and space potentials.

The air model facility described in Appendix 8.3, used to evaluate line bend calculation curves, is practical for substations as well. This facility has the advantage of using commercially available 60-Hz power supplies and field measuring equipment. Air models operating at high frequency (24 kHz) have also been used with satisfactory results (11).

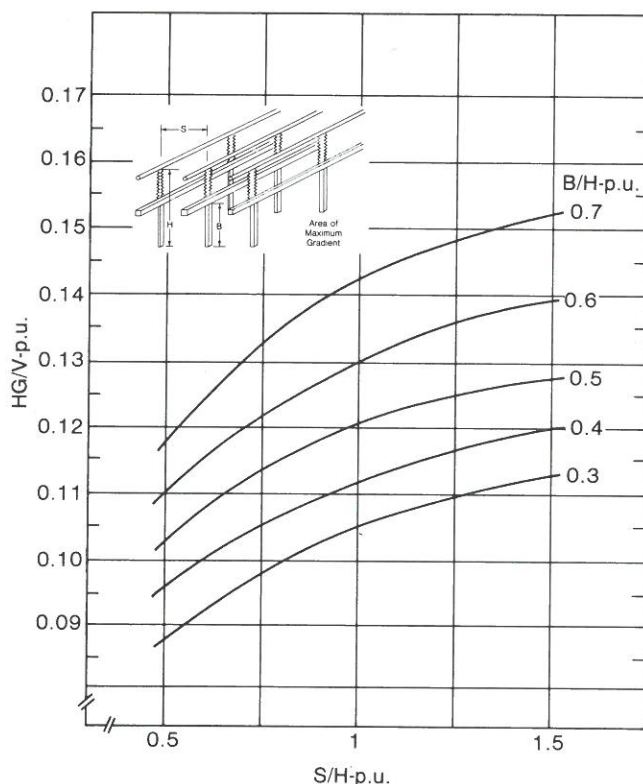


Figure 8.3.26. Generalized curves to calculate the maximum gradient at ground close to substation buses with grounded bases.

8.4 CALCULATION OF MAGNETIC FIELDS

GENERAL METHOD FOR TRANSMISSION LINES

The magnetic field of transmission lines is calculated using a two-dimensional analysis assuming parallel lines over a flat earth. Using the coordinate system described in Figure 8.4.1, where the axis, Z , is parallel to the line, the magnetic field strength, $H_{j,i}$, at point (x_i, y_i) at a distance, $r_{i,j}$, from a conductor with a current, I_i , has an amplitude

$$H_{j,i} = \frac{I_i}{2\pi r_{i,j}} \quad (8.4.1)$$

In vectorial notation,

$$\vec{H}_{j,i} = \frac{\vec{I}_i \times \vec{r}_{j,i}}{2\pi r_{i,j}^2} = \frac{I_i}{2\pi r_{i,j}} \vec{\phi}_{i,j} \quad (8.4.2)$$

where $\vec{\phi}_{i,j}$ is the unit vector in the direction of the product of the vector current and the vector segment $\vec{r}_{i,j}$. The unit vector is equal to:

$$\vec{\phi}_{i,j} = -\frac{y_i - y_j}{r_{i,j}} \vec{u}_x + \frac{x_i - x_j}{r_{i,j}} \vec{u}_y \quad (8.4.3)$$

where \vec{u}_x and \vec{u}_y are the unit vectors in the direction of horizontal and vertical axes, respectively.

The total magnetic field is the sum of all the contributions from line currents:

$$\vec{H}_j = \sum_i \frac{I_i}{2\pi r_{i,j}} \vec{\phi}_{i,j} \quad (8.4.4)$$

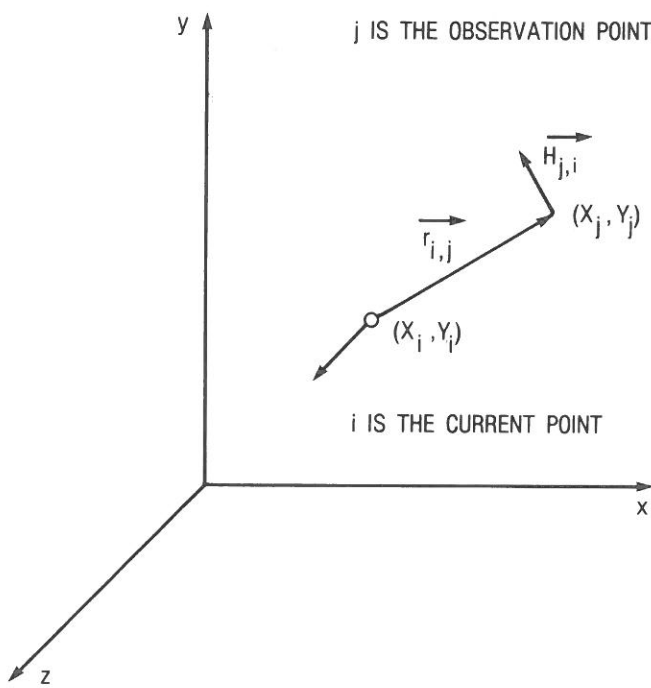


Figure 8.4.1. Coordinate system for magnetic-field calculations.

The magnetic flux density is

$$\vec{B} = \mu \vec{H} \quad (8.4.5)$$

where $\mu = 4\pi 10^{-7}$ H/m for both air and ground.

In most practical cases, the magnetic field in proximity to balanced three-phase lines may be calculated considering the currents in the conductors and in the ground wires and neglecting earth currents. The magnetic field is affected by the presence of earth return currents especially at large distances from the line. These currents are distributed in the earth for balanced three-phase systems, for which the total earth return current is zero. Earth return is taken into account using Carson's equations (24). However, this approach is awkward because of the infinite series in Carson's mutual impedance equations. A more intuitive approach is presented in Appendix 8.5. The magnetic field produced by each conductor and its earth return is expressed by Eq. 8.4.6, derived in Appendix 8.5:

$$\vec{H}_{j,i} = \frac{I_i}{2\pi r_{i,j}} \vec{\phi}_{i,j} - \frac{I_i}{2\pi r'_{i,j}} \left[1 + \frac{1}{3} \left(\frac{2}{\gamma r'_{i,j}} \right)^4 \right] \vec{\phi}'_{i,j} \quad (8.4.6)$$

The first term is the same as that in Eq. 8.4.2 and is sufficient for calculation of the magnetic field in proximity to the line, up to 100 m in the example of Table 8.4.1. The second term represents a correction factor that accounts for earth return currents:

$$\gamma = [j\omega\mu(\sigma + j\omega\epsilon)]^{1/2} \quad (8.4.7)$$

where σ is the earth conductivity ($\sigma \approx 0.001$ to 0.02 S/m) and ϵ is the earth permittivity ($\epsilon \approx 8.85 \cdot 10^{-12}$, the same as air permittivity, may be used). Equation 8.4.8 shows that $r'_{i,j}$ is also a complex number:

$$r'_{i,j} = \left[\left(x_i - x_j \right)^2 + \left(y_i + y_j + \frac{2}{\gamma} \right)^2 \right]^{1/2} \quad (8.4.8)$$

The complex operator, $\vec{\phi}'_{i,j}$, is shown in Eq. 8.4.9:

$$\vec{\phi}'_{i,j} = - \left[\frac{y_i + y_j + 2/\gamma}{r'_{i,j}} \right] \vec{u}_x + \frac{x_i - x_j}{r'_{i,j}} \vec{u}_y \quad (8.4.9)$$

The result of Eq. 8.4.6 is a complex value, indicating that the magnetic field, H , is not in phase with the conductor current when the earth resistivity is taken into account.

Using Eq. 8.4.6, the total magnetic field at the point (x,y) is obtained summing the contribution of the currents in all the conductors ($i = 1, n$), including ground wires. The result of Eq. 8.4.6 is a complex number that may be characterized by its vector components along the x and y axes:

$$\begin{aligned} H_x &= H_{x,r} + jH_{x,i} \\ H_y &= H_{y,r} + jH_{y,i} \end{aligned} \quad (8.4.10)$$

Or, the number may be described by the real and imaginary vectors:

$$\begin{aligned} \vec{H}_r &= H_{x,r} \vec{u}_x + H_{y,r} \vec{u}_y \\ \vec{H}_i &= H_{x,i} \vec{u}_x + H_{y,i} \vec{u}_y \end{aligned} \quad (8.4.11)$$

The magnitude and direction of the axes of the magnetic field ellipse may be calculated using a procedure similar to that described for the electric field in Section 8.3.

EXAMPLE CALCULATION

The magnetic-field intensity was calculated for the base case 800-kV line configuration presented in Table 3.2.1. The results are shown in Tables 8.4.1 and 8.4.2 and in Figure 8.4.2.

Table 8.4.1
EXAMPLE OF CALCULATION OF
MAGNETIC FIELD AT GROUND LEVEL

| Distance From Line Center (m) | Field Component Due to Conductor Currents (A/m) | Field Component Due to Earth Currents (A/m) | Total Field |
|-------------------------------|---|---|-------------------------|
| 0 | 14.34 | .117 $\times 10^{-1}$ | 14.3 |
| 70 | 1.530 | .118 $\times 10^{-1}$ | 1.531 |
| 100 | 0.762 | .119 $\times 10^{-1}$ | 0.763 |
| 700 | 0.157 $\times 10^{-1}$ | .144 $\times 10^{-1}$ | 0.243 $\times 10^{-1}$ |
| 1000 | 0.772 $\times 10^{-2}$ | .811 $\times 10^{-2}$ | 0.1143 $\times 10^{-1}$ |
| -1000 | 0.772 $\times 10^{-2}$ | .819 $\times 10^{-2}$ | 0.1150 $\times 10^{-1}$ |
| 10 ⁴ | 0.772 $\times 10^{-4}$ | .778 $\times 10^{-4}$ | 0.146 $\times 10^{-4}$ |

Line: 800-kV base case of Table 3.2.1, flat configuration,
phase spacing 14 m, conductor height 18.5 m
Conductor currents: $I_A = -1000 - j1732$ A, $I_B = 2000$ A, $I_C = -1000 + j1732$ A

Table 8.4.2
MAGNETIC FIELD AT POINT X = 0, Y = 0

| | Horizontal Component (A/m) | Vertical Component (A/m) | Major Axis | |
|---------------------------|--|------------------------------------|-----------------|--------------|
| | | | Amplitude (A/m) | Phase (Deg.) |
| Without earth return | 6.26 | -j 14.3 | 14.34, | 0 |
| Earth return contribution | -0.98×10^{-4} $+j 0.11 \times 10^{-3}$ | -0.012 $+j 0.49 \times 10^{-3}$ | 0.012, | -91 |
| Total field | 6.26 $+j 0.11 \times 10^{-3}$ | -0.012 $-j 14.3$ | 14.34, | 0.03 |

Up to 100 m from the line, a small distance compared with the earth return current depth, the earth return currents have a negligible effect on the magnetic field caused by the line, as shown in Table 8.4.1 and in Table 8.4.2.

In the skin depth region, there is a combination of the conductor current field and of the earth current field that tends to increase the combined field. Beyond distances comparable to the earth return current depth, the two field components cancel each other significantly. It should also be noted that the total field is slightly greater on the side where the outer phase with current lagging the current of the center phase is located (see Table 8.4.1 for distances of + and -1000 m).

The maximum ground level magnetic field occurs at the center of the line and is $H_{\max} = 14 \text{ A/m}$, which corresponds to a flux density:

$$B = \mu H = 4\pi 10^{-7} \cdot 14 = 1.76 \cdot 10^{-5} \text{ Wb/m}^2 = 0.176 \text{ gauss.}$$

For comparison, the earth magnetic field is about 0.5 gauss. It should be noted, however, that the earth field is not time-varying, whereas the line field varies with power frequency.

The major axis of the rotating vector is horizontal at the center of the line and tilts to 45° at about 14 m from the line center.

Practical measurements of magnetic fields under transmission lines have often shown significant deviations from calculated values for a number of reasons. The magnetic field is very sensitive to line current unbalance, which is usually not measured accurately. Induced current on shield wires, counterpoises, and extraneous currents in the nonhomogeneous earth influence the magnetic field in ways that cannot be accurately calculated. Finally, lines often show significant deviations not included in the infinitely long, uniform line assumption.

8.5 MEASUREMENT OF ELECTRIC FIELDS

TECHNIQUES FOR THE MEASUREMENTS OF THE UNPERTURBED ELECTRIC FIELD

The theory and operational characteristics of electric-field meters and the techniques for their calibration and use are described in detail in a study on electrostatic and electromagnetic effects of transmission lines (3). The instrument used at Project UHV (see Figure 8.5.1) is of the self-contained, free-body type, which is the most commonly used for measurement of transmission-line fields. It measures the 60-Hz, induced current or charge oscillating between two halves of an insulated conductive body (free-body) in an electric field. The theory of the free-body field meter is described in Appendix 8.2. This meter is convenient for outdoor measurements near HV transmission lines or substations because it is portable, it allows measurements anywhere above the ground plane, and it does not require a known ground reference. Meters of this type are calibrated to read the rms value of the electric-field component along a main axis at the power frequency (either 60 Hz or 50 Hz). Unless otherwise specified, the main axis of the instrument should correspond to its electrical axis, i.e., the axis of greatest sensitivity to the electric field.

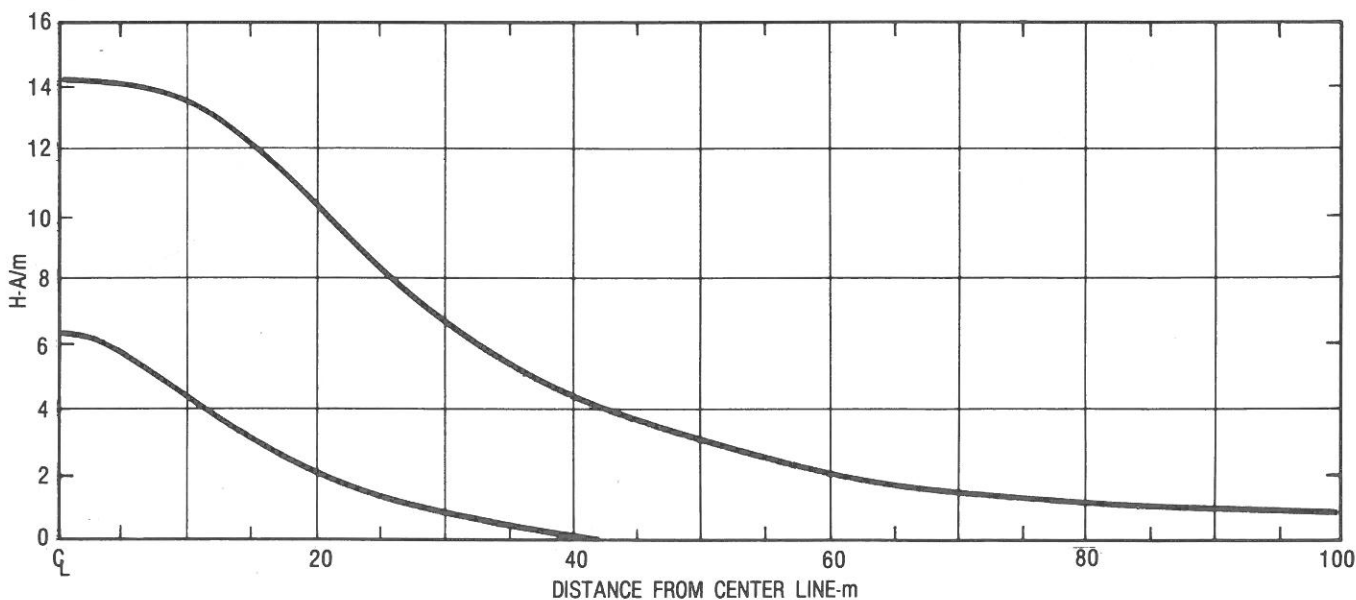


Figure 8.4.2. Magnetic-field intensity. Magnitudes of the major and minor axes of the field ellipse.



Figure 8.5.1. Measurement of the unperturbed electric field near ground.

Calibration of the meter is best accomplished by introducing it in a region of known uniform field such as that produced by parallel plates. At Project UHV, parallel plates with a stretched metal screen on a 3×3 -m frame with a 1-m separation have been employed with satisfactory results. The calibration setup is shown in Figure 8.5.2. Grading rings, to which potentials are applied using a resistive divider, are employed to grade the field at the perimeter of the structure and to provide isolation from surrounding perturbations. To further reduce the effect of surrounding grounded structures and the possible effect of meter handle leakage, both plates are energized using a center-tapped transformer, as shown in Figure 8.5.2, so that the center of the space between the plates remains at ground potential.

Another calibration method is to measure the current induced on a conducting plate of known area on a flat ground. Although this method is less accurate than the parallel plate method, it is convenient for transmission-line work because it employs the ac field generated by the line itself. Figure 8.5.3 shows the details of a flat plate used at Project UHV. A 1×1 -m panel in the center of the plate is insulated from the rest of the plate and connected to ground through an ammeter. The rest of the plate acts as a guard ring.

For a 1-m^2 area, the surface charge is numerically equal to the average displacement charge over the area:

$$q = D = \epsilon_0 E \quad (8.5.1)$$

The current from the panel to ground is

$$I = \frac{dq}{dt} = j\omega\epsilon_0 E \quad (8.5.2)$$

For 60-Hz fields in air

$$\omega = 377 \text{ rad/s}$$

and

$$\epsilon_0 = 8.85 \cdot 10^{-12} \text{ F/m}$$

Substituting these numerical values in Eq. 8.5.2 and solving for E yields

$$E = 3.10^8 I \text{ V/m} \quad (8.5.3)$$

If I is the rms value of the measured current, E is the rms value of the electric field perpendicular to the surface. For best accuracy, the center panel should be a little less than 1 m^2 . The air gap to the guard ring must have the edges of the metal precisely aligned on the flat plane so that the displacement flux is divided equally in the gap. The effective area of the center panel equals that of the center panel plus one-half of the area of the gap. The guard ring should extend in width at least five times the height of the panel above the virtual ground. The virtual ground may be much below the surface of dry gravel, dry macadam, or the like. To minimize field distortion, the meter should be kept close to the panel but no closer than a distance equal to the maximum meter dimensions, and the operator must kneel.

The procedure recommended by the IEEE (1) for measuring the lateral profile of the electric field of transmission lines consists of holding the meter at a height of 1 m above ground at a distance of at least 2.5 m (8 ft) from the operator. Usually, however, only small errors are encountered, even at 1.5 m from the operator. In its vertical position the meter measures the vertical component of the electric field. To perform measurements along other directions, the meter should be rotated. Measurements in the plane of the field ellipse require that the observer-meter line be parallel to the conductors. Rotation about this line, which coincides with the handle, will permit the determination of the maximum and minimum field components (semi-axes of the field ellipse) and their directions. The meter measures the (perturbed) field correctly at points close to an object provided that the electrical center of the meter is well defined and that the distance between the meter and the object is greater than the largest meter dimension.

The usual accuracy of practical outdoor electric-field measurements is near 10%, but in controlled conditions it is easily better than 5%. The accuracy is limited by a number of factors: distortion of the field by the body of the person holding the handle, conductivity of the handle (especially in the presence of moisture), reading errors, temperature effects, and difficulty in positioning the electric center of the meter at the point of measurement and in positioning the electric axis of the meter along the direction of measurement.

To check for handle leakage, the electric field should be oriented with its axis perpendicular to the plane of the electric field ellipse, where zero electric field should be measured. A reading of the meter in this position, expressed in percentage of the maximum field, would represent the order of magnitude of the error caused by handle leakage. If the harmonic content of the electric field is significant, an additional measuring error may result because of the different response of the field meter to different frequencies.

Comparisons between measured and calculated electric field profiles are affected not only by measurement errors but also by the simplifications usually made for the calculations, such as the assumption of flat ground and the absence of any object. If the ground is not flat, the field close to ground will be enhanced by hills and reduced by valleys. If the ground is irregular or if there is tall grass, a virtual average ground should be assumed for the calculations, and measurements should be made away from any protuberance. Nearby objects such as trees and houses will reduce the field at ground of three-phase lines, often by a significant amount (see Section 8.17).

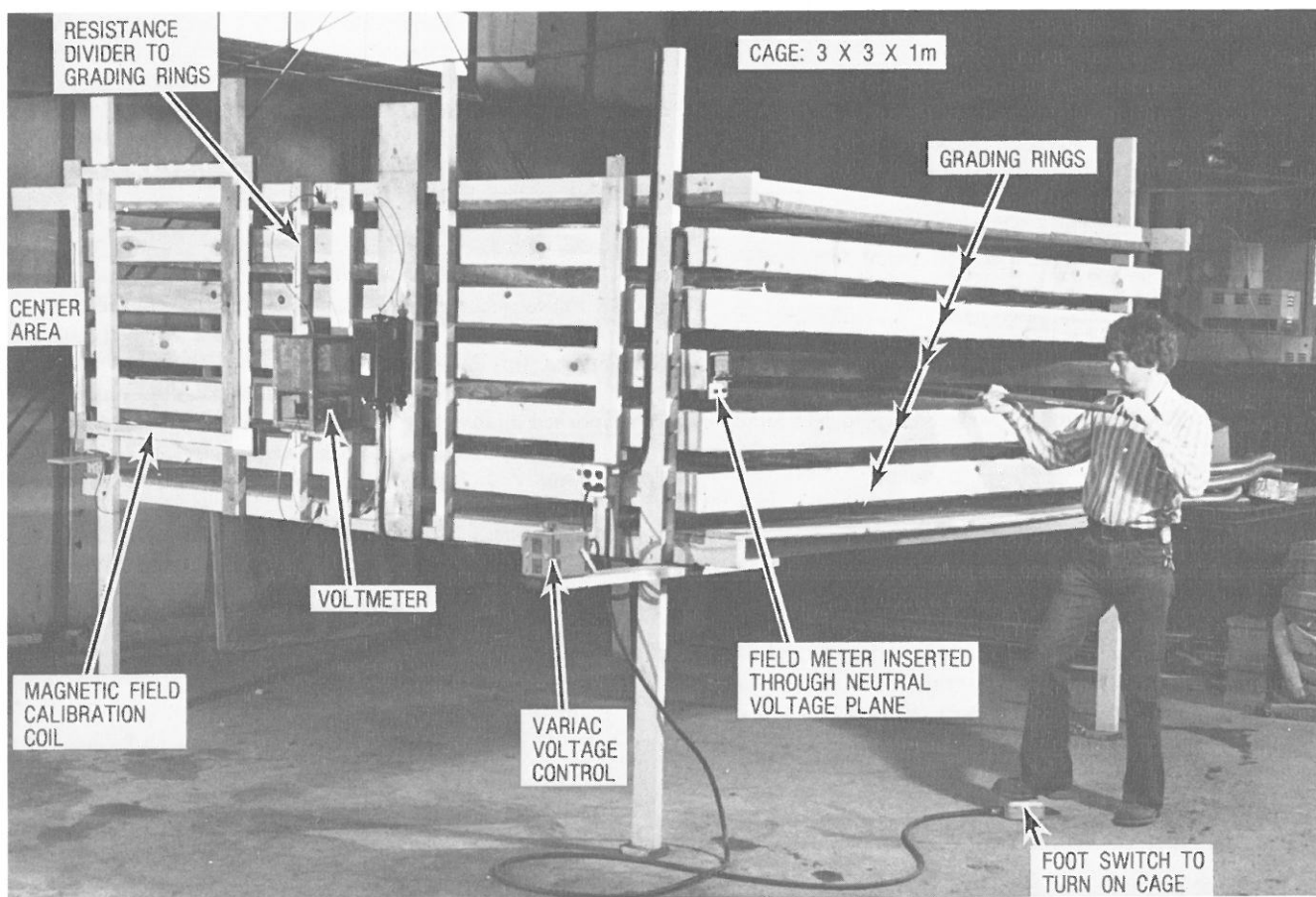
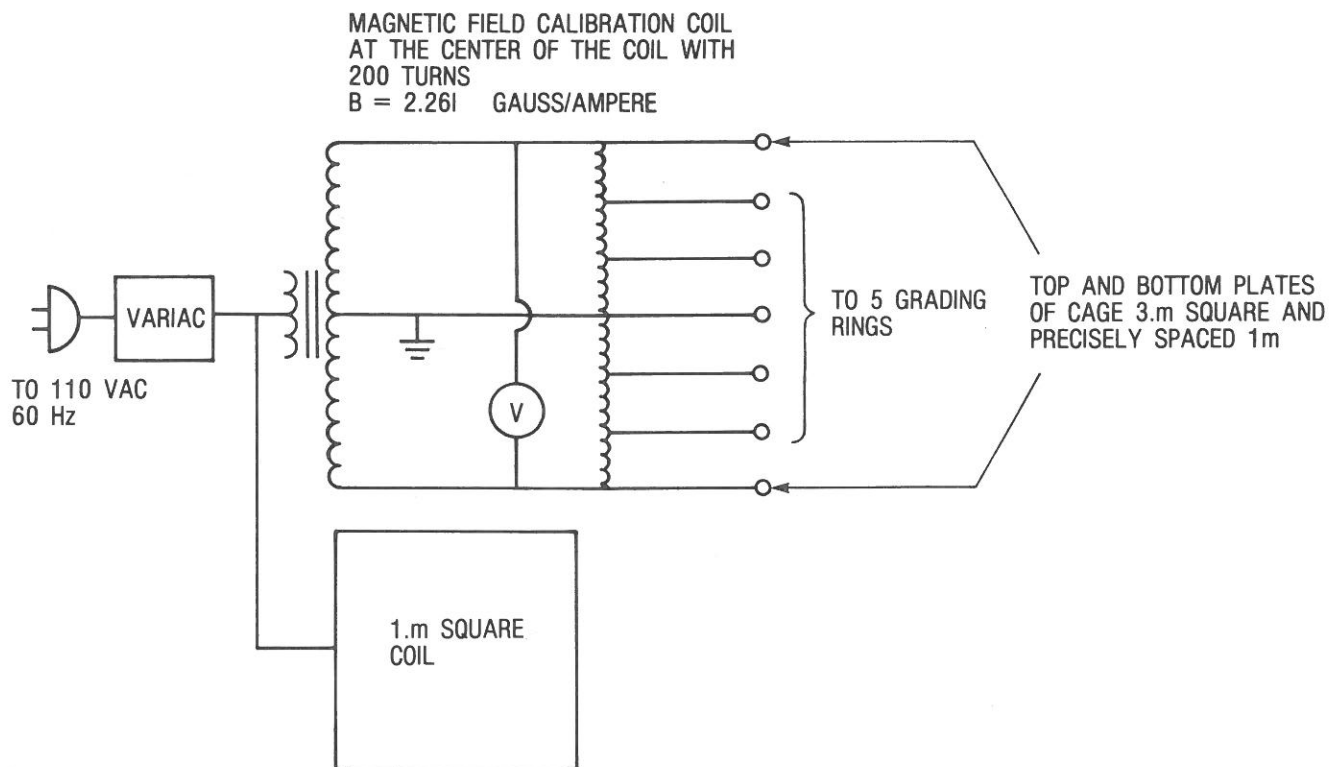


Figure 8.5.2. Parallel plate setup for calibration of electric-field meters.

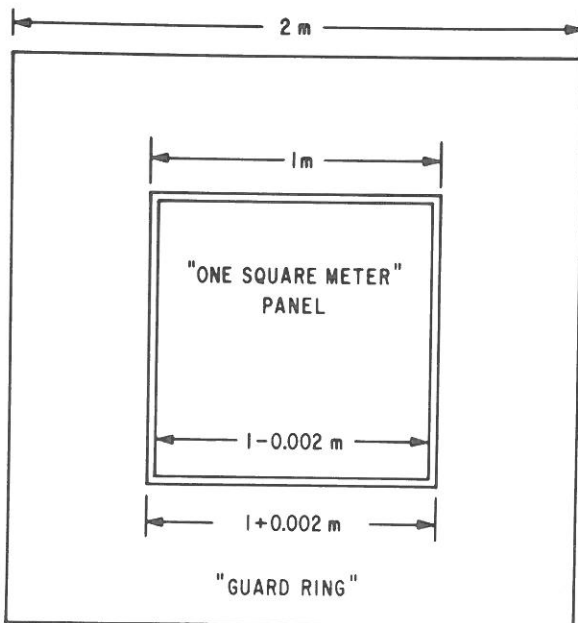
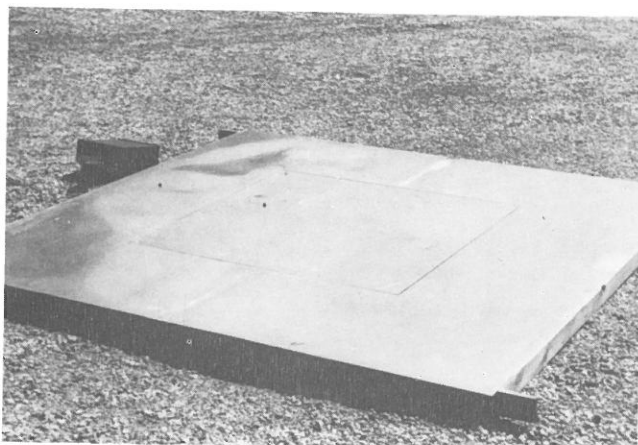


Figure 8.5.3. Flat plate with a one square meter panel for electric-field meter calibration.

MEASUREMENTS OF THE ELECTRIC FIELD ON A BOUNDARY SURFACE

The field, E , on a boundary surface may be determined by measuring the current, I , induced in a known area, S , and using

$$I = 2\pi f \epsilon E S \quad (8.5.4)$$

where f is the frequency and ϵ the dielectric constant of air. An example of application is the measurement of the electric field at ground by means of a flat plate, as shown in the preceding subsection. The technique used for more complex surfaces is shown in Figure 8.5.4. The current is measured from a small square of copper foil surrounded by more copper foil that acts as a guard ring. A coaxial cable, with its shield connected to the guard ring and grounded, is used to connect the sensor to the ammeter.

MEASUREMENT OF THE SPACE POTENTIAL

The space potential is a very useful parameter for characterizing the induction by electric fields in tall vertical objects,



Figure 8.5.4. Measurement of electric field on a boundary surface.

which are often in nonuniform electric fields. Hence, a suitable technique has been developed for measuring space potential, as shown in Figure 8.5.5. The space-potential probe consists of a calibrated probe grounded through a shielded wire. The current induced in the probe and measured by the ammeter carried by the operator is proportional to the space potential. In fact, for a given shape and area of a probe, the current induced is

$$I_{\text{probe}} = k \cdot [(V_{\text{sp}} - V_{\text{probe}}) + L \cdot E] \quad (8.5.5)$$

where k is a coefficient of proportionality, V_{sp} is the unperturbed space potential, V_{probe} is the voltage of the probe, L is a characteristic dimension of the probe, and E is the unperturbed electric field. The characteristic dimension of a sphere of radius R is $L = 3R$, and the coefficient $k = \omega \cdot 4\pi\epsilon R$. For probes of small dimensions with respect to the distance to ground ($L \cdot E \cdot \ll V_{\text{sp}}$) and grounded ($V_{\text{probe}} = 0$), Eq. 8.5.5 may be simplified to

$$I_{\text{probe}} = k V_{\text{sp}} \quad (8.5.6)$$

The shielded cable connecting the probe to the ammeter is assumed to cause a negligible disturbance to the induced current. The effects of the shape of the probe and of the shielded cable are accounted for during the calibration of the space-potential probe. A simple calibration of the space-potential probe is accomplished by inserting the probe in a shielded room, e.g., the

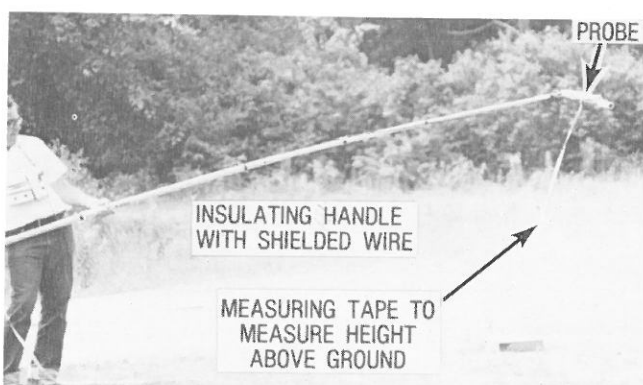


Figure 8.5.5. Measurement of the unperturbed space potential.

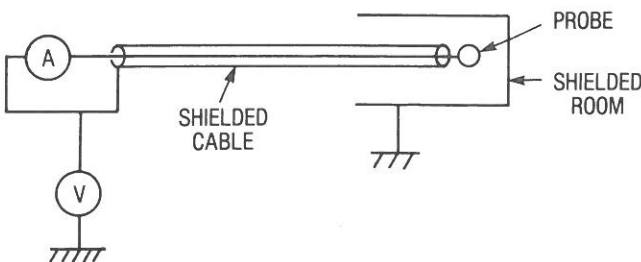


Figure 8.6.6. Schematic diagram of the calibration of a space-potential probe.

space between the parallel plates used to calibrate the field meter (see Figure 8.5.2), and applying a known voltage, e.g., 100 V, to the entire measuring system (probe, shielded cable, ammeter), as shown in Figure 8.5.6. The reading of the ammeter divided by the applied voltage gives the constant, k , to use in Eq. 8.5.6.

8.6 MEASUREMENTS OF MAGNETIC FIELDS

The ac magnetic field (B -field) at power frequency may be measured with a shielded coil probe, as shown in Figure 8.6.1 (8).

The sensor coil may be oriented to measure the horizontal, vertical, or maximum magnitude of the field. The presence of the operator's body does not alter the magnetic field nor does the presence of the meter and adapter box, made of nonmagnetic materials (see Figure 8.6.1). Magnetic-field probes are calibrated by introducing the probe in a magnetic field of known magnitude and direction. A reference magnetic field may be conveniently generated by a coil 1 × 1 m in size with about 10 to 100 turns, as shown in Figure 8.5.2. For the setup of Figure 8.5.2, the current obtained from a 110-V receptacle was limited by a 100-W light bulb. The magnetic flux density, B , is calculated by integrating Ampere's law

$$B = \mu H = \mu \int dH = \mu \int \frac{I}{4\pi r^2} \vec{r} \times d\vec{L} \quad (8.6.1)$$

where $\mu = 4\pi \cdot 10^{-7}$ H/m is the permeability of air, r is the distance from the element, dL , of the coil to the point of measurement, and I is the current in the coil.

Equation 8.6.1 may be used to calculate the magnetic field in the centers of coils of different shapes and with N number of terms:

for a square coil of side equal to $2r$:

$$B_{\text{center}} = \frac{NI}{r} \cdot \frac{\sqrt{2}}{\pi} \quad (8.6.2)$$

for a circular coil of radius r :

$$B_{\text{center}} = \frac{NI}{r} \cdot 0.5 \quad (8.6.3)$$

for long parallel wires with separation equal to $2r$:

$$B_{\text{center}} = \frac{NI}{r} \cdot \frac{1}{\pi} \quad (8.6.4)$$



Figure 8.6.1. Measurement of the magnetic field.

The SI unit of measurement of the magnetic flux density, B , is the Tesla (T) or Weber per square meter (Wb/m²). The commonly used CGS unit is the gauss (G). 1 T = 10⁴ G.

The lateral profile of the magnetic field of a transmission line should be measured at 1 m above ground, as is the electric-field profile. The probe should be oriented for the maximum reading. The magnetic field is generally not perpendicular to the ground, and the vertical component of the field is generally not coincident with the maximum field.

8.7 COMPARISON BETWEEN HV TRANSMISSION-LINE AND COMMON ENVIRONMENT ELECTRIC AND MAGNETIC FIELDS

Examples of maximum electric field at ground level are tabulated in Table 8.7.1. In practical situations, trees, bushes, distribution lines, and structures all reduce the maximum electric field to the measured actual electric field at ground level.

Only a few examples of the magnetic field are given in Table 8.7.1 because the magnetic field is of little concern and is seldom measured. Line currents are always changing with load. The resulting magnetic-field fluctuations are difficult to correlate with line-current load fluctuations at a specific time.

Measured common environment electric fields are shown in Tables 8.7.2 and 8.7.3. Touching appliances for short exposure times and sitting under lamps for long exposure times appear to be the most significant common environment electric-field induction situations.

Table 8.7.1
EXAMPLES OF MAXIMUM GROUND-LEVEL ELECTRIC FIELDS TO BE FOUND UNDER POWER TRANSMISSION LINES

| Line Voltage | Maximum Field at Ground Level |
|------------------------|-------------------------------|
| 23 kV, 3-phase | 10-50 V/m |
| 23 kV, 1-phase | 10-25 V/m |
| 115 kV | 0.1-2 kV/m |
| 345 kV | 2.3 kV/m |
| 345 kV | 5 kV/m |
| 345 kV, double circuit | 5.6 kV/m |
| 500 kV | 8 kV/m |
| 765 kV | 10 kV/m |

Note: The first four lines of the table refer to actual measurements made in Pittsfield, Mass. The last four lines refer to calculated values for existing lines.

Table 8.7.2
**MEASUREMENTS OF ELECTRIC AND MAGNETIC FIELDS
 ABOUT PROJECT UHV**

| | | | |
|---|---------|-------|--|
| Old garage room | | | |
| 30 cm from 220 V heater power cord | 0.2 | V/cm | |
| 30 cm from lightswitch wire | 0.23 | V/cm | |
| 30 cm from ceiling lamp | 0.05 | V/cm | |
| Workshop | | | |
| 30 cm from drill cord | 0.25 | V/cm | |
| 30 cm from unshielded fluorescent lamp | 0.35 | V/cm | |
| Computer room | | | |
| 30 cm from plotter | 0.1 | V/cm | |
| 30 cm from telephone | 0.1 | V/cm | |
| 30 cm from light bulb | 0.05 | V/cm | |
| Conference room | | | |
| In projection booth | 0.5 | V/cm | |
| 30 cm from large metal ungrounded clock | 0.5 | V/cm | |
| Hallway | | | |
| 30 cm from incandescent lamp | 0.1 | V/cm | |
| 30 cm from ungrounded emergency light | 0.2 | V/cm | |
| Control room | | | |
| 30 cm from ungrounded emergency light | 0.2 | V/cm | |
| Reversed plug | 0.4 | V/cm | |
| 30 cm from air conditioner | 0.03 | V/cm | |
| 30 cm from TV, set off | 0.12 | V/cm | |
| 30 cm from TV, set on | 0.15 | V/cm | |
| 30 cm from line cords | 0.3 | V/cm | |
| Middle of room | >0.0005 | V/cm | |
| Kitchen | | | |
| 30 cm from incandescent lamp | 0.05 | V/cm | |
| Next to large 30 cup coffee maker | 0.7 | V/cm | |
| Reversed plug | 0.3 | V/cm | |
| 3 cm above 1000 W stove coil | 1.12 | gauss | |
| 20 cm above 1000 W stove coil | 0.078 | gauss | |

Table 8.7.3
**MEASUREMENTS OF ELECTRIC AND MAGNETIC FIELDS
 IN SINGLE-FAMILY RESIDENCE**

| | | |
|---|---------|-------|
| Outside the building | 0.0005 | V/cm |
| | 0.00001 | gauss |
| Under electric service drop | 0.00002 | gauss |
| Kitchen—center of room | 0.00006 | gauss |
| | 0.006 | V/cm |
| 20 cm from iron | 0.75 | V/cm |
| 20 cm from refrigerator | 0.7 | V/cm |
| 20 cm from mixer #1 | 1.2 | V/cm |
| mixer #2 | 0.4 | V/cm |
| 30 cm above a 110 V cord to mixer | 0.4 | V/cm |
| 20 cm above rotisserie | 0.1 | V/cm |
| above rotisserie, reverse plug | 3.0 | V/cm |
| above rotisserie, power on | 0.14 | gauss |
| Living room—center of room | 0.00017 | V/cm |
| | 0.00006 | gauss |
| Bathroom—center of room | 0.001 | V/cm |
| | 0.00006 | gauss |
| Electric razor | 0.014 | gauss |
| Over sink with lights | 0.5 | V/cm |
| Den—center of room under overhead light | 0.03 | V/cm |
| | 0.00005 | gauss |
| Next to lamp | 0.4 | V/cm |
| Next to lamp cord | 0.00005 | gauss |
| | 0.0001 | gauss |

8.8 ELECTRIC-FIELD INDUCTION ON OBJECTS

INTRODUCTION

The electric-field induction on objects in proximity to high-voltage conductors energized at power frequencies may be characterized by the following parameters:

- The short-circuit current I_{sc} , which is the rms value of the current induced in a zero impedance connection between object and ground
- The rms value of the voltage induced between object and ground, V_{og} , which depends on the insulation between object and ground
- The impedance between object and ground

$$Z_{og} = V_{og}/I_{sc} \quad (8.8.1)$$

- The capacitance of object to ground, C_{og}
- The spark-discharge capacitance to ground, C_s , which has a negligible series resistance in the spark-discharge time of 1 microsecond
- The maximum energy stored per half-cycle in the object

$$J = \frac{1}{2} C_s (\sqrt{2} V_{og})^2 = C_s V_{og}^2 \quad (8.8.2)$$

TRANSMISSION-LINE INDUCED CURRENTS

The calculation of the electric induction caused by a source of electric field on an object is extremely complicated. Calculation can be simplified considerably, as shown in Appendix 8.4, if:

- The source of induction is represented by the induced unperturbed electric field (for objects close to ground level) or space potential (for objects high above ground).
- The effect of the object's presence on the charge of the energized electrodes is ignored.

The current induced in objects close to ground is

$$I_{sc} = j \omega \epsilon E S \quad (8.8.3)$$

I_{sc} is the current that would flow in a short-circuit connection between object and ground; $\omega = 2\pi f$ where f is the power frequency; E is the vertical component of the unperturbed electric field at ground level; and S is the equivalent charge-collecting area of the object.

CURRENT INDUCED ON A SPHERE ABOVE GROUND

A sphere of radius r at height h above ground in an unperturbed field of value E has an induced current

$$I_{sc} = j \omega V_{sp} \frac{4\pi E}{\frac{1}{r} - \frac{1}{2h}} \quad (8.8.4)$$

$$= j \omega \epsilon E h \frac{4\pi}{\frac{1}{r} - \frac{1}{2h}} = j \omega \epsilon E h S$$

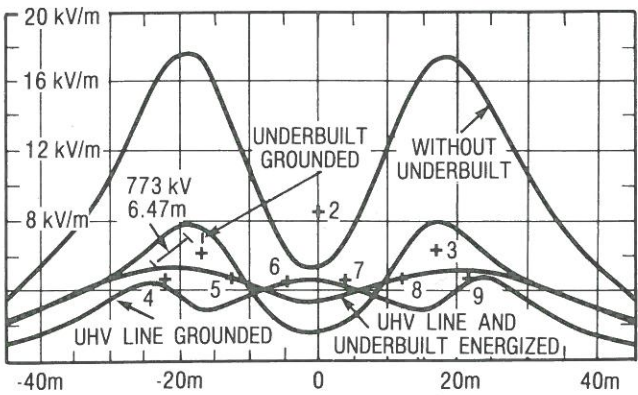


Figure 8.17.20. Double-circuit 240-kV lines (conductors 4 to 9) built under a 1200-kV line (conductors 1, 2, 3). Phase of conductors 4 and 9 is the same as conductor 2. Phase of conductors 5 and 7 is the same as conductor 3. Phase of conductors 6 and 8 is the same as conductor 1. Equivalent radii: 45 cm for the 1200-kV line and 40 cm for the 240-kV lines.

One of the most severe drawbacks of this type of complex transmission-line design is the increase in conductor-surface gradient and the consequent increase in audible and radio noise. The increase in audible noise of the UHV line is significant, requiring a more expensive line design. Furthermore, the design of the underbuilt itself requires particular attention because of corona. To be effective in reducing the field at ground and corona on the conductors, underbuilt lines require three or four subconductors with large spacing, even for relatively low voltages. For instance, the line of Figure 8.17.20 at 240 kV requires bundles of three conductors of 3.8 cm diameter, spaced 0.7 m.

Practical Considerations: The design of an underbuilt line for electric-field reduction of a UHV line must consider many different problems related to construction and operation. The Tennessee Valley Authority (TVA) has 500-kV lines under

which short sections of 161-kV lines were built for the purpose of conserving right-of-way. Although these lines were not built with the intent to reduce the electric field, they provide a source of practical information applicable to UHV lines with lower-voltage underbuilt lines to cancel electric fields. An example of 500-kV lines with underbuilts is shown in Figure 8.17.21.

Work on the underbuilt or on the higher-voltage line while the other line is energized is very difficult. Therefore, both transmission lines must be deenergized to service one line. Currents coupled from the higher-voltage line for ground faults may interfere with the lower-voltage underbuilt power system relaying. Finally, the lower-voltage line may experience a higher than normal lightning tripout rate because of the lower insulation coupled with a higher than normal tower height. However, the higher-voltage line will effectively shield the underbuilt from direct strokes.

Appendix 8.1 CALCULATION OF MAXIMUM FIELD

The maximum phasor component of the electric (or magnetic) field in a point in space is represented by the magnitude and direction of the major semi-axis of the field ellipse. The ellipse axes correspond to the zero rate of change of the field magnitude with respect to angle in space or with respect to time. Both methods are presented in this appendix. The angle derivation starts with the vertical and horizontal components expressed by Eqs. 8.3.12 and 8.3.13.

The magnitude, E_α , of the component of the field along a direction defined by an angle, α , with respect to the horizontal is expressed by Eq. A8.1.1:

$$(E_\alpha)^2 = (E_{ry} \sin \alpha + E_{rx} \cos \alpha)^2 + (E_{iy} \sin \alpha + E_{ix} \cos \alpha)^2 \quad (\text{A8.1.1})$$

To determine the angles corresponding to maximum and minimum fields, the derivative of expression Eq. A8.1.1 with respect to the angle α is set equal to zero:

$$\frac{d(E_\alpha)^2}{d\alpha} = 0 \quad (\text{A8.1.2})$$

Equation A8.1.2, after suitable manipulations, may be written as a quadratic equation with $\tan \alpha$ as the unknown variable:

$$\begin{aligned} \tan^2 \alpha (E_{ry} \cdot E_{rx} + E_{iy} \cdot E_{ix}) + \tan \alpha (-E_{iy}^2 + E_{ix}^2 \\ - E_{ry}^2 + E_{rx}^2) - (E_{ry} \cdot E_{rx} \\ + E_{iy} \cdot E_{ix}) = 0 \end{aligned} \quad (\text{A8.1.3})$$

Equation A8.1.3 has two solutions corresponding to the major and minor axes of the ellipse. The magnitude of the semi-axes is evaluated by substituting the angles into Eq. A8.1.1.

The time derivation starts with the vertical and horizontal components expressed as vectors with instantaneous values varying in time:

$$\vec{E}_x = H \cos(\omega t + \theta) \cdot \vec{u}_x \quad (\text{A8.1.4})$$

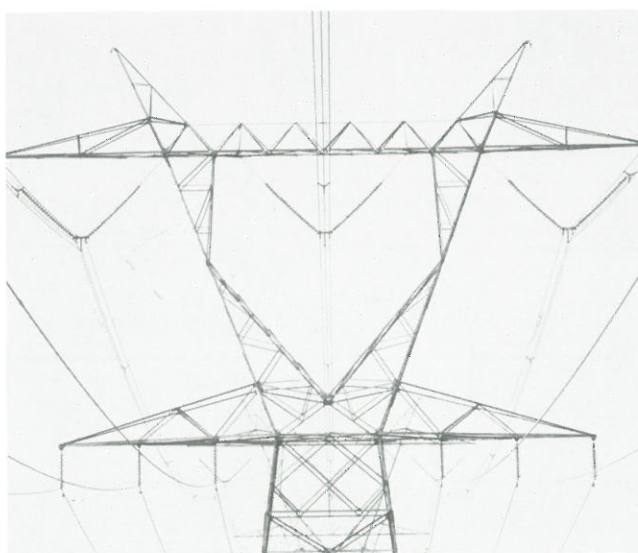


Figure 8.17.21. Tower with 500-kV line and two underbuilt 161-kV lines (TVA).

and

$$\vec{E}_y = V \cos(\omega t + \phi) \cdot \vec{u}_y \quad (\text{A8.1.5})$$

Where

H is the maximum horizontal component

$$H^2 = E_{rx}^2 + E_{ix}^2$$

θ is the phase angle of the horizontal component

$$\theta = \arctan \frac{E_{ix}}{E_{rx}}$$

V is the maximum vertical component

$$V^2 = E_{ry}^2 + E_{iy}^2$$

and ϕ is the phase angle of the vertical component

$$\phi = \arctan \frac{E_{iy}}{E_{ry}}$$

The instantaneous field is a vector in space expressed by

$$\vec{E} = \vec{E}_x + \vec{E}_y \quad (\text{A8.1.6})$$

The square of the instantaneous field magnitude is

$$E^2 = H^2 \cos^2(\omega t + \theta) + V^2 \cos^2(\omega t + \phi) \quad (\text{A8.1.7})$$

The field is maximum or minimum when

$$\frac{dE^2}{dt} = 0 \quad (\text{A8.1.8})$$

The solution of Eq. A8.1.8 is

$$\tan(2\omega t) = - \frac{H^2 \sin 2\theta + V^2 \sin 2\phi}{H^2 \cos 2\theta + V^2 \cos 2\phi} \quad (\text{A8.1.9})$$

If ωt_1 is a solution of Eq. A8.1.9, the other solutions are

$$\omega t_m = \omega t_1 + (m - 1)\pi/2 \quad (\text{A8.1.10})$$

There are four solutions for $m = 1$ to 4 . The pair, t_1, t_3 (and t_2, t_4), corresponds to two directions of the same axis. The magnitudes of the semi-axes are evaluated by substituting these terms into Eq. A8.1.7.

Appendix 8.2 MEASUREMENT OF ELECTRIC FIELD WITH A FREE-BODY METER

A portable electric-field meter is shown in Figure A8.2.1. The device measures the current flowing between the top half and the bottom half of the box. This current provides the surface charge terminating the displacement flux, $D = \epsilon E$, on the constant potential of the conductive aluminum box. For practical reasons, this meter is not shaped as a sphere. Therefore, the derivation included in this appendix is applied with an estimated equivalent radius for the practical box constructed.

A calibration of the meter with a known field provides a method of evaluating the radius of the equivalent sphere. A geometry trim adjustment is provided to calibrate this meter.

The portable field tester is treated as a sphere in a uniform field because this approach has a tractable solution.

The distribution of surface charge on a conducting sphere in a uniform Laplacian field is evaluated by assuming a Legendre polynomial in the form of a spherical harmonic series as follows:

$$\varphi = \sum_{n=0}^{\infty} (A_n r^n + B_n r^{-n-1}) [C_n P_n \cos \theta + D_n Q_n \cos \theta] + C \quad (\text{A8.2.1})$$

The boundary conditions are interpreted from the uniform far field as

$$\varphi_p = -Er \cos \theta + \varphi_o \quad (\text{A8.2.2})$$

The near field around the sphere is sketched in Figure A8.2.2.

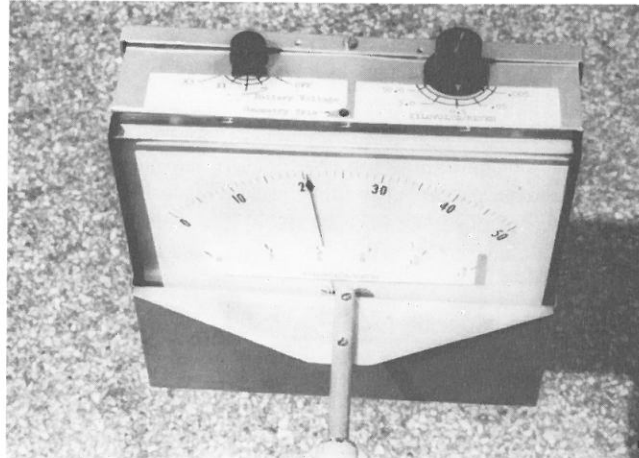


Figure A8.2.1. Free-body electric field meter.

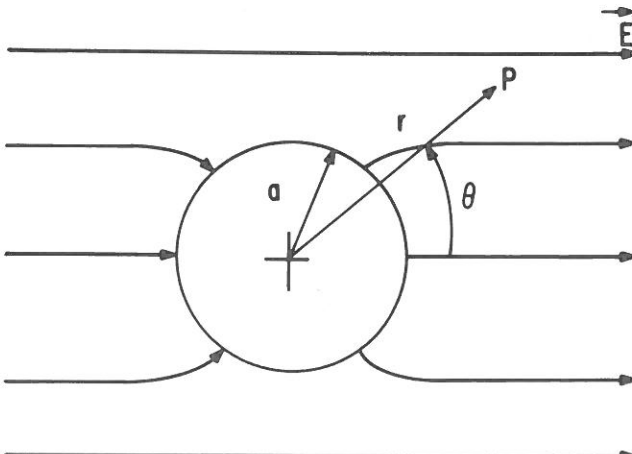


Figure A8.2.2. The boundary condition.

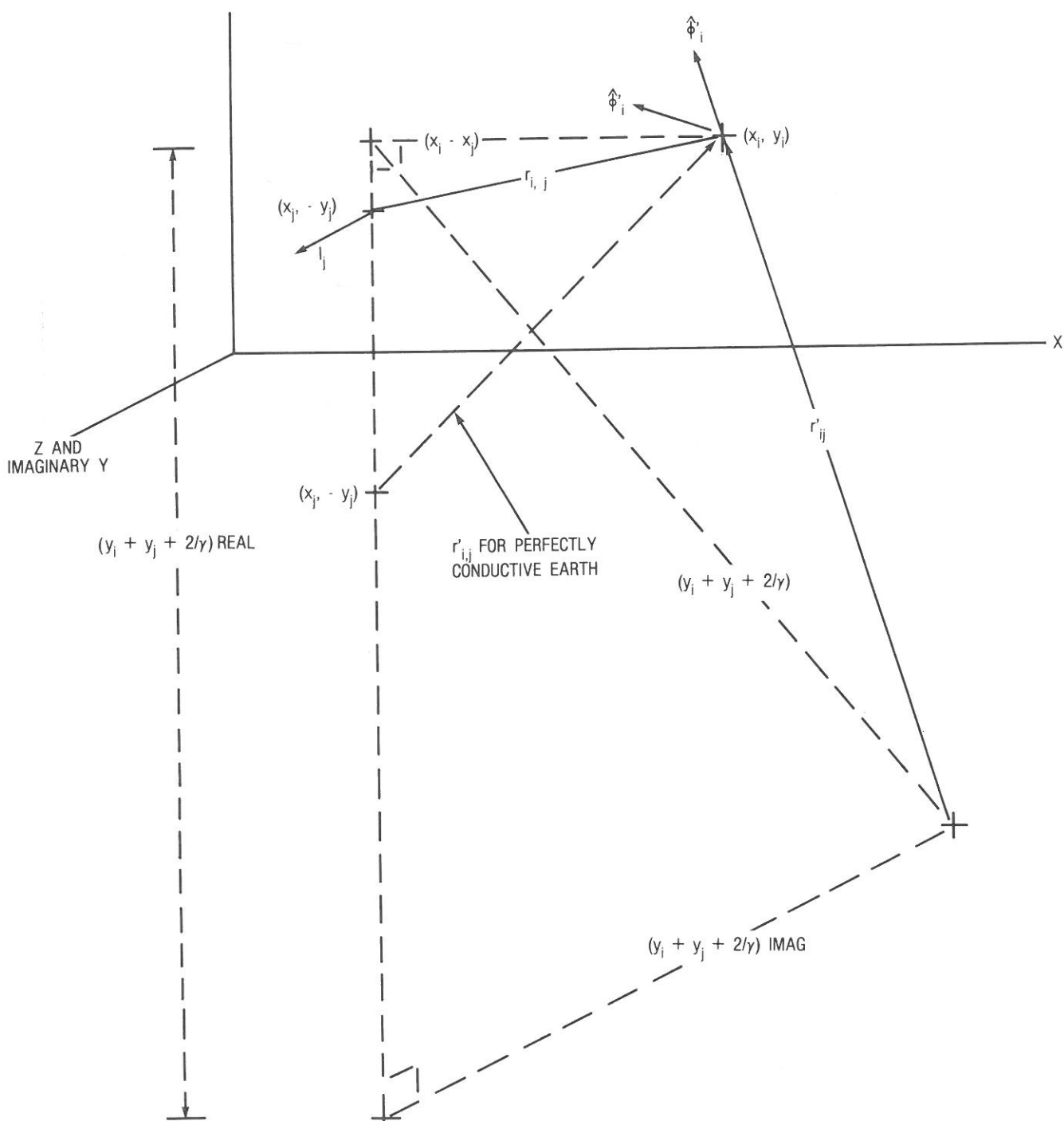


Figure A8.5.1. Coordinate system for complex distance mutual impedance with earth return.

References

General

- 8.1 IEEE Working Group. "Electrostatic Effects of Overhead Transmission Lines, Pt. I—Hazards and Effects," *IEEE Transactions on Power Apparatus and Systems*, Vol. PAS-91, pp. 422–426, March/April 1972.
- 8.2 IEEE Working Group. "Electrostatic Effects of Overhead Transmission Lines, Pt. II—Methods of Calculation," *IEEE Transactions on Power Apparatus and Systems*, Vol. PAS-91, pp. 426–444, March/April 1972.

8.3 D. W. Deno, L.E. Zaffanella. *Electrostatic and Electromagnetic Effects of Ultrahigh-Voltage Transmission Lines*, Palo Alto, Calif.: Electric Power Research Institute, June 1978, EPRI Research Project 566-1, Final Report, EL-802.

8.4 L.E. Rogers, R.O. Gilbert, J.M. Len, T.D. Bracken. "BPA 1100 kV Transmission System Development—Environmental Studies," *IEEE Transactions on Power Apparatus and Systems*, Vol. PAS-98, pp. 1958–1967, Nov/Dec 1979.

8.5 D.E. Perry, V.L. Chartier, G.L. Reiner. "BPA 1100 kV Transmission System Development—Corona and Electric Field Studies," *IEEE Transactions on Power Apparatus and Systems*, Vol. PAS-98, pp. 1728–1738, Sept/Oct 1979.

8.6 H.A. Kornberg. "Concern Overhead," *EPRI Journal*, June/July 1977, pp. 6-13.

Electric and Magnetic Fields, Calculations, and Measurements

8.7 D.W. Deno. "Transmission Line Fields," *IEEE Transactions on Power Apparatus and Systems*, Vol. PAS-95, pp. 1600-1611, Sept/Oct 1976.

8.8 Working Group on Electrostatic and Electromagnetic Effects of Transmission Lines. "Measurement of Electric and Magnetic Fields from Alternating Current Power Lines," *IEEE Transactions on Power Apparatus and Systems*, Vol. PAS-97, pp. 1124-1131, July/Aug 1978.

8.9 T.D. Bracken. "Field Measurements and Calculations of Electrostatic Effects of Overhead Transmission Lines," *IEEE Transactions on Power Apparatus and Systems*, Vol. PAS-76, pp. 494-504, March/April 1976.

8.10 J.D. Placido, C.H. Shih, B.J. Ware. "Analysis of the Proximity Effects in Electric Field Measurements," *IEEE Transactions on Power Apparatus and Systems*, Vol. PAS-97, pp. 2167-2177, Nov/Dec 1978.

8.11 S.A. Sebo. *Model Study of Electric Field—Effects on Substations*, Palo Alto, Calif.: Electric Power Research Institute, January 1978, Ohio State University, EPRI Project RP753, Final Report, EL-632.

8.12 C.H. Shih, J.D. Placido, B.J. Ware. "Analysis of Parallel Plate Simulation of the T/L E-Field as Related to Biological Effects Laboratory Studies," *IEEE Transactions on Power Apparatus and Systems*, Vol. PAS-96, pp. 962-968, May/June 1977.

8.13 K.G. Lowstrand, "Determination of Exposure to Electric Fields in Extra High Voltage Substations," *Scan. J. Work Env. & Health*, 3(1976), pp. 190-198.

8.14 U.S. Department of Energy. National Bureau of Standards. *AC Transmission Line Field Measurements*, Publication HCP/T-6010/E1, Washington, D.C.: Government Printing Office, Nov 1977.

Electric and Magnetic Field Induction in Objects

8.15 D.W. Deno. "Calculating Electrostatic Effects of Overhead Transmission Lines," *IEEE Transactions on Power Apparatus and Systems*, Vol. PAS-93, pp. 1458-1471, Sept/Oct 1974.

8.16 J. Patrick Reilly. "Electric Field Induction on Sailboats and Vertical Poles," *IEEE Transactions on Power Apparatus and Systems*, Vol. PAS-97, pp. 1373-1383, July/Aug 1978.

8.17 D.W. Deno, "Electrostatic Effects Induction Formulas," *IEEE Transactions on Power Apparatus and Systems*, Vol. PAS-94, No. 5, pp. 1524-1536, September/October 1975.

8.18 P. Sarma Maruvada, N. Hylten-Cavallius. "Capacitance Calculations for Some Basic High Voltage Electrode Configurations," *IEEE Transactions on Power Apparatus and Systems*, Vol. PAS-94, pp. 1708-1713, Sept/Oct 1975.

8.19 J.P. Reilly, "An Approach to the Realistic Case Analysis of Electric Field Induction From AC Transmission Lines," Third International Symposium on High-Voltage Engineering, Milan, Italy: August 1979.

8.20 J.G. Rene, R.P. Comsa. "Computer Analysis of Electrostatically Induced Currents on Finite Objects by EHV Transmission Lines," *IEEE Transactions on Power Apparatus and Systems*, Vol. PAS-87, pp. 997-1002, April 1968.

8.21 J.D. Tranen, G.L. Wilson. "Electrostatically Induced Voltages and Currents on Conductive Objects Under EHV Transmission Lines," *IEEE Transactions on Power Apparatus and Systems*, Vol. PAS-90, pp. 768-775, March/April 1971.

8.22 G.L. Reiner. "Electrostatic Effects Near HVAC Transmission Lines. Field Tests and Computer Results," *IEEE Transactions on Power Apparatus and Systems*, Vol. PAS-72, p. 1729, July/Aug 1972.

8.23 J.P. Reilly. "Electric Field Induction on Long Objects. A Methodology for Transmission Line Impact Studies," *IEEE Transactions on Power Apparatus and Systems*, Vol. PAS-98, pp. 1841-1852, Nov/Dec 1979.

8.24 J.R. Carson. "Wave Propagation in Overhead Wires with Ground Return," *Bell Syst. Tech. Jour.*, 1926, Vol. 5, pp. 539-554.

8.25 D.E. Hedman. "Propagation on Overhead Transmission Lines II. Earth Effects and Practical Results," *IEEE Transactions on Power Apparatus and Systems*, Vol. PAS-84, pp. 205-211, March 1965.

8.26 A. Taflove, J. Dabkowski. "Prediction Method for Buried Pipeline Voltages Due to 60 Hz AC Inductive Coupling," *IEEE Transactions on Power Apparatus and Systems*, Vol. PAS-98, pp. 780-794, May/June 1979.

8.27 A. Taflove, M. George, J. Dabkowski. "Mitigation of Buried Pipeline Voltage Due to 60 Hz AC Inductive Coupling," *IEEE Transactions on Power Apparatus and Systems*, Vol. PAS-98, pp. 1806-1823, Sept/Oct 1979.

8.28 J. Dabkowski, A. Taflove. *Mutual Design Considerations for Overhead AC Transmission Lines and Gas Pipelines*, Palo Alto, Calif.: Electric Power Research Institute, September 1978, Report EL-904.

Electric Field Induction in People

8.29 C.F. Dalziel. "Electric Shock Hazard," *Spectrum*, February 1972, pp. 41-50.

8.30 C.F. Dalziel. "The Effect of Electric Shock on Man," *IRE Transactions on Medical Electronics*, CPGME-5, May 1956.

8.31 C.F. Dalziel. "Re-evaluation of Lethal Electric Currents," *IEEE Transactions on Industry and General Applications*, 4:467-76, October 1968.

8.32 C.F. Dalziel, W.R. Lee. "Lethal Electric Currents," *Spectrum*, February 1969, pp. 44-50.

8.33 L.E. Geddes, L.E. Baker. "The Specific Resistance of Biological Material—A Compendium of Data for the Biomedical Engineer and Physiologist," *Med. & Biol. Engng.*, Vol. 5, pp. 271-293, Pergamon Press, 1967.

8.34 IEEE Working Group on Electrostatic and Electromagnetic Effects. "Electric and Magnetic Field Coupling from High Voltage AC Power Transmission Lines—Classification of Short-Term Effects on People," *IEEE Transactions on Power Apparatus and Systems*, Vol. PAS-97, pp. 2243-2252, Nov/Dec 1978.

8.35 D.W. Deno. "Currents Induced in the Human Body by High Voltage T/L Electric Field—Measurement and Calculation of Distribution and Dose," *IEEE Transactions on Power Apparatus and Systems*, Vol. PAS-96, No. 5, pp. 1517-1527, September/October 1977.

8.36 K.H. Schneider, and others. *Displacement Currents to the Human Body Caused by the Dielectric Field Under Overhead Lines*, CIGRE, 1974 Session, Report 36-04.

8.37 J.E. Bridges, M.J. Frazier. *The Effects of 60 Hz Electric and Magnetic Fields on Patients with Implanted Cardiac Pacemakers*, Palo Alto, Calif.: Electric Power Research Institute, September 1979, EPRI Project 673-1, Final Report, EA-1174.

Biological Effects of Electric and Magnetic Fields

8.38 W.B. Kouwenhoven, O.R. Langworthy, M.L. Singewald, G.G. Knickerbocker. "Medical Evaluation of Man Working in AC Electric Fields," *IEEE Transactions on Power Apparatus and Systems*, pp. 506-511, 1967.

8.39 T. Takagi, T. Muto. "Influences Upon Human Bodies and Animals of Electrostatic Induction Caused by 500 kV Transmission Lines," *Electrical Engineering (Japan)*, February 1971.

8.40 V.P. Korobkova, and others. *Influence of the Electric Field in 500 and 750 kV Switchyards on Maintenance Staff and Means for Its Protection*, CIGRE, Institute of Electrical & Electronics Engineers, 1972 Session, Report 23-06.

8.41 *Study in the USSR of Medical Effects of Electric Fields on Electric Power Systems*, 1978 Special Publication No. 10, IEEE—PES. 78 CHO 1020-7-PWR.

8.42 R.D. Phillips. "Biological Effects of High Strength Electric Fields on Small Laboratory Animals," Battelle Annual Report March 1978, Prepared for DOE.

- 8.43 Battelle, "Effects of Electric Fields on Large Animals," Fourth Interim Report EPRI EA-331, Research Project 799, February 1979.
- 8.44 B. Greenberg. *The Effect of High Voltage Transmission Lines on Honey Bees*, Palo Alto, Calif.: Electric Power Research Institute, October 1978, EPRI Project 334-1, EA-841.
- 8.45 J.W. Bankoske, T.J. Reed, G.W. McKee, H.B. Graves, and D.T. Poznaniak. *Some Biological Effects of High Intensity, Low Frequency (60 Hz) Electric Fields on Small Birds and Animals*, Palo Alto, Calif.: Electric Power Research Institute, December 1977, EPRI Research Project RP 129, Final Report.
- 8.46 H.B. Graves, et al. "Perceptibility and Electrophysiological Response of Small Birds to Intense 60 Hz Electric Fields," *IEEE Transactions on Power Apparatus and Systems*, Vol. PAS-97, pp. 1070-1073, July/Aug 1978.
- 8.47 "Research on the Biological Effects of Electric and Magnetic Fields," *Revue Generale D' L'electricite Numero Special*, July 1976.
- 8.48 IIT Research Institute, "Evaluation of Health and Environmental Effects of Extra High Voltage (EHV) Transmission," May 1978, Prepared for U.S. Environmental Protection Agency, Contract No. 68-01-4604.
- 8.49 IIT Research Institute, "Biological Effects of High Voltage Electric Fields: An Update," EPRI EA-1123, Vol. 1 & 2, Project 857-1, Final Report, July 1979.
- 8.50 Richard D. Phillips, Wm. T. Kaune, "Biological Effects of Static and Low Frequency Electro-Magnetic Fields: An Overview of United States Literature," Battelle, BNWL-2262, April 1977.
- 8.51 J.E. Bridges, "Biological Effects of High Voltage Electric Fields: State-of-the-Art Review and Program Plan," IITRI, Nov. 1975, EPRI Project 381-1, Final Report NTIS No. PB-247-454.
- 8.52 J.E. Bridges. "Environmental Considerations Concerning the Biological Effects of Power Frequency (50 or 60 Hz) Electric Fields," *IEEE Transactions on Power Apparatus and Systems*, Vol. PAS-97, Jan/Feb 1978.
- 8.53 G.E. Atoian. "Are There Biological and Psychological Effects Due to Extra High Voltage Installations?" *IEEE Transactions on Power Apparatus and Systems*, Vol. PAS-97, No. 1, Jan/Feb 1978.
- 8.54 B. Knave, et al. "Long-Term Exposure to Electric Fields, A Cross-Sectional Epidemiological Investigation of Occupationally Exposed Workers in High Voltage Substations," *Electra*, No. 65, June 1980.
- 8.55 M.V. Strumza. "Influence sur la Sante Humaine de la Proximite des Conducteurs d'Electricite a Haute Tension. Resultats D'Une Enquete Sur La Consommation Medicale," *Arch. Mal. Prof.* 31:6, 1970, pp. 269-276.
- 8.56 F. Roberge. "State of Health of Maintenance Electricians Engaged in the Maintenance of Hydro Quebec 735 kV Stations," *Hydro Quebec Report*, May 1976.
- 8.57 Marcel DeVizio. "Evaluation of the Effects of the Electric Field on Lineman Working on a 735 kV Tower in the Vicinity of Energized Conductors," *Joint Meeting of the Construction Methods and Equipment Section and Transmission Section Canadian Electrical Assoc.*, Montreal, Quebec, March 1977.
- 8.58 W. Janischewskyj, J.G. Stopps. "Assessment of Exposure to Electric Fields of Personnel Working on AC Transmission Systems, as part of an Epidemiological Study," *Canadian Electrical Association*, Vancouver, B.C., March 1979.
- 8.59 A.R. Sheppard, M. Eisenbud. *Biological Effects of Electric and Magnetic Fields of Extremely Low Frequency*, New York: New York University Press, 1977.
- 8.60 *Proceedings of the Biomagnetic Effects Workshop*, Lawrence Berkeley Laboratory, April 1978, LBL-7452.
- 8.61 J.D. Grissett, and others. *Exposure of Primates for One Year to Electric and Magnetic Fields Associated with ELF Communications Systems*, Pensacola, Fla.: Naval Aerospace Medical Research Laboratory, November 1977, NAMRL-1240.
- 8.62 D.E. Beischer and others. *Exposure of Man to Magnetic Fields Alternating at Extremely Low Frequency*, Pensacola, Fla.: Naval Aerospace Medical Research Laboratory, 1973, NAMRL-1180.
- 8.63 J.D. Grissett, et al. *Data Supplement to Interim Research Report*, Pensacola, Fla.: Naval Aerospace Medical Research Laboratory, June 1976, NAMRL-1225.
- 8.64 J. de Lorge. *A Psychobiological Study of Rhesus Monkeys Exposed to Extremely Low Frequency—Low Intensity Magnetic Fields*, Pensacola, Fla.: Naval Aerospace Medical Research Laboratory, NAMRL-1203. (Available from NTIS as AD 000078.)
- 8.65 Mantell. "Untersuchungen über die Wirkung eines Magnetischen Wechselfeldes 50 Hz auf den Menschen," Inaugurale Dissertation zur Erlangung der Medizinischen Doktorwürde der medizinischen Fakultät der Albert Ludwig Universität, 1975.

Fuel Ignition

- 8.66 B. Lewis, G. Van Elbe. *Combustion, Flames and Explosives of Gases*, New York: Academic Press, Inc., 1951.
- 8.67 A.R. Boyle, F.J. Llewellyn. "The Electrostatic Ignitability of Various Solvent Vapor Air Mixtures," *Society of the Chemical Industry Journal*, 66, March 1947, pp. 99.
- 8.68 H.F. Calcate, C.A. Gregory, et al. "Spark Ignition Effect of Molecular Structure," *Industrial and Engineering Chemistry*, November 1952.
- 8.69 A.H. McKinney. "Electrical Ignition of Combustible Atmospheres," *ISA Transactions*, Vol. 1, No. 1, pp. 45-64, January 1962.
- 8.70 Ontario Hydro. *Electrostatic Induction Near EHV Transmission Lines Are Related to the Hazards of Handling Gasoline*, Ontario Hydro, November 1963, Report No. 63-391.
- 8.71 H.J. West, D.W. McMullan. "Fire Induced Flashovers of EHV Transmission Lines," *IEEE-PES Winter Meeting*, New York, Paper A 73 047-2, February 1978.

Poles in High Intensity Fields

- 8.72 G.G. Hespelt. "Pole Fires and Nonmetallic Ground-Wire Fasteners," *IEEE Summer Meeting*, Mexico City, Paper A 77 673-7, July 1977.
- 8.73 G.E. Lusk, S.T. Mak. "EHV Wood Pole Fires: Their Cause and Potential Cures," *IEEE Transactions on Power Apparatus and Systems*, Vol. PAS-95, pp. 621-629, March/April 1976.
- 8.74 G.E. Lusk. "Reducing Fires on EHV Wood Poles," *Electrical World*, September 15, 1975.

Shielding Methods

- 8.75 D.W. Deno. "UHV Transmission Line Electric Field Reduction With a Set of Horizontal Wires," *IEEE Transactions on Power Apparatus and Systems*, Vol. PAS-96, pp. 1507-1516, Sept/Oct 1977.
- 8.76 F.G. Kaidanov (NIPT). "The Protection of Substation Personnel Against the Influence of Electrical Fields," *Soviet Power Engineering*, No. 1, Jan 1974.

Selection of Clearances

- 8.77 Institute of Electrical & Electronics Engineers. *National Electric Safety Code*, 1977 Edition, ANSI C2, New York: IEEE, Inc.
- 8.78 R.S. Gens, E.H. Gehrig, R.B. Eastvedt. "BPA 1100 kV Transmission System Development Planning, Program, and Objectives," *IEEE Transactions on Power Apparatus and Systems*, Vol. PAS-98, Nov/Dec 1979.
- 8.79 W.R. Rish, M.C. Morgan. "Regulating Possible Health Effects from AC Transmission Line Electromagnetic Fields," *Proceedings of the IEEE*, Vol. 67, No. 10, Oct 1979, pp. 1416-1427.
- 8.80 Y.I. Lyskov, Y.S. Emma, M.D. Stolarov. "Electrical Field as a Parameter Considered in Designing Electric Power Transmission of 750-1150 kV," *USA-USSR Symposium on Ultrahigh Voltage Transmission*, Washington, D.C. 1976.